

AD-783 700

LASER DOPPLER VELOCIMETER EVALUATION
AND MEASUREMENTS IN A FLOW WITH DRAG
REDUCTION

Peter David Fitzgerald

Michigan University

Prepared for:

Office of Naval Research

1974

DISTRIBUTED BY:

NTIS

National Technical Information Service

U. S. DEPARTMENT OF COMMERCE

5285 Port Royal Road, Springfield Va. 22151

AD783700

DDC

CH

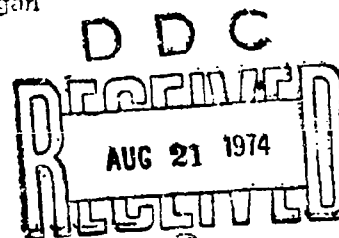
1

LASER DOPPLER VELOCIMETER EVALUATION
AND
MEASUREMENTS IN A FLOW WITH DRAG REDUCTION

by

Peter David Fitzgerald

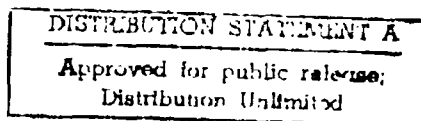
A dissertation submitted in partial fulfillment
of the requirements for the degree of
Doctor of Philosophy
(Naval Architecture and Marine Engineering)
in The University of Michigan
1974



Doctoral Committee:

Professor William P. Graebel, Co-Chairman
Professor Horst G. Nowacki, Co-Chairman
Professor Richard B. Couch
Professor William W. Willmarth

Reproduced by
NATIONAL TECHNICAL
INFORMATION SERVICE
U. S. Department of Commerce
Springfield, VA 22151



*Approved for public release,
distribution unlimited*

84

ACKNOWLEDGMENTS

The author would like to express his appreciation to the members of his dissertation committee for their assistance during the course of this research.

Mr. Ben E. Bourland and Mr. Stern S. Morgan contributed greatly to this work both in their technical support and in their warm friendship.

Many thanks go to the author's colleagues Mr. R.J. Staples and Dr. A.M. Lindrose for their helpful suggestions and discussion as well as their constant encouragement. A grateful acknowledgment is extended to the many other individuals who contributed in innumerable ways to the author's deeper appreciation of science and life.

And lastly, the author would like to especially thank Ms. Miriam Klammer and Ms. Diana Erbe for their patient and thorough effort in typing this manuscript.

This work was made possible with financial support from several sources, among them the Fluid Dynamics Branch of the Office of Naval Research, the Horace H. Rackham School of Graduate Studies, the Department of Naval Architecture and Marine Engineering, and the Department of Applied Mechanics and Engineering Science.

TABLE OF CONTENTS

ACKNOWLEDGMENTS	ii
LIST OF TABLES	iv
LIST OF FIGURES	v
CHAPTER	
I. INTRODUCTION	1
II. THE FLOW SYSTEM	9
General Description	
Polymer Preparation and Injection	
Scattering Particle Considerations	
III. THE OPTICAL SYSTEM	16
Description of Optical System	
Test Volume Size	
Signal-to-Noise and Broadening Considerations	
IV. THE SIGNAL PROCESSING SYSTEM	35
The Frequency Tracker	
Frequency Tracker Evaluation	
V. MEASUREMENTS AND OBSERVATIONS IN A POLYMER FLOW	50
Drag Reduction Degradation Studies	
Velocity Profile Results	
VI. CONCLUSIONS	68
APPENDIX	70
REFERENCES	75

LIST OF TABLES

Table	Page
3.1 Properties of Scattered Particles Used	28
5.1 Drag Reduction Parameters	53
5.2 Values of the Friction Factor (F) for Fresh Water at $R_N = 5 \cdot 10^4$	55
5.3 Percent Drag Reduction as a Function of Passes Through the System for $R_N = 4 \cdot 10^4$	57
5.4 Percent Drag Reduction as a Function of Passes Through the System for $R_N = 5 \cdot 10^4$	58
5.5 Percent Drag Reduction as a Function of Passes Through the System for $R_N = 6 \cdot 10^4$	59

LIST OF FIGURES

Figure	Page
2.1 Flow System10
3.1 Typical Reference Beam System17
3.2 Typical Dual-Scatter System19
3.3 Two-Component Optical Geometry20
3.4 Receiving Optics Layout23
3.5 Dependence of S/N on Detector Aperture and Effective Number of Particles for the Dual-Scatter and Reference Beam Modes33
4.1 Signal Processing Arrangement36
4.2 Frequency Tracker Schematic38
4.3 Tracker Evaluation Circuitry45
4.4 A Real Doppler Signal and the Response of the Frequency Tracker to S/N on a Simulated Doppler Signal46
4.5 Frequency Tracker Response to Simulated Pseudo-Random Modulation and Real Doppler Modulation47
5.1 Maximum Drag Reductions for Low-Polymer Concentrations54
5.2 Axial Mean Velocity Profiles at $R_N = 5 \cdot 10^4$63
5.3 Experimental Dimensionless Polymer Velocity Profiles66
A.1 Wide Band Amplifier71
A.2 Balanced Mixer72
A.3 Frequency Discriminator and Tracker73
A.4 Hybrid Active Filter74

CHAPTER I

INTRODUCTION

Turbulent friction reduction, caused by the addition of low concentrations of certain high molecular weight polymers to a fluid like water, is still unexplained, although there is agreement that alteration of the region very near the wall, the viscous sublayer, plays a major role in the drag-reduction phenomenon. Barker (1973), for example, with measurements on a free turbulent jet, supported the hypothesis that the polymer induced drag reduction is not related to any effects on the free jet but rather it is related to some effect very near the boundary layer wall.

For lack of sufficient theoretical explanation of the basic mechanism of the turbulent structure in drag reducing flows, most of the studies in this area have had to rely heavily on experimental work. These experiments have been performed with one of the following approaches: 1) pressure drop versus flow rate or gross flow studies; 2) mean velocity profile measurements; and 3) turbulence intensity measurements. From these studies, many proposals and theories about the structure of the flows have been presented. A review of these models is presented by Kumar and Sylvester (1973).

So-called displacement models, in which the law of the wall is displaced upwards, but parallel to, the Newtonian curve for increasing percentages of drag reduction have been proposed by several authors. Of particular interest are the two and three-layer models employed to

describe the flow structure.

A two-layer model was proposed by Seyer and Metzner (1969). It consists of a turbulent core region and a viscous sublayer extended to its intersection with the law-of-the-wall resulting, therefore, in a thickened viscous sublayer relative to the Newtonian fluid case. Virk et al. (1970), among others, proposed a three-layer model. His model was comprised of a viscous sublayer, an elastic sublayer and a turbulent region similar to the two-layer model. This model describes the mean flow structure at low drag reduction and when integrated predicts friction factor results consistent with the maximum drag reduction data of Seyer and Metzner.

As Kumor and Sylvester (1973) point out, the displacement models should be considered low drag reduction models because results from high drag reduction experiments indicate an increase in slope of the velocity profile in the turbulent core region, and therefore a decrease in the mixing length constant. This would therefore negate the hypothesis that the law-of-the-wall is shifted upwards, but parallel to, the Newtonian curve.

Lurley (1967) is among those who suggest that molecular extension and molecular entanglement resist the formation of the streamwise vortices as well as absorbing energy from the turbulent eddies. Gadd (1966) and Walsh (1967) hypothesize that turbulence dissipation is not the mechanism involved in drag reduction, but rather, that a resulting reduction in the generation of turbulence is responsible.

To date the only studies that have specifically investigated the wall-region in drag reducing flows have been those by Eckelman, Fortuna, and Hanratty (1972) and Donohue, Tiederman, and Reischman (1972).

Eckelman et al. used electrochemical techniques to show that the addition of drag-reducing polymers caused an increase in the average wavelength of flow oriented eddies close to the wall. Their model, however, did not allow for changes in the burst rate of low momentum streaks (Willmarth and Lu, 1972, among others, have shown that in Newtonian flows the cycle of turbulence production includes large-scale intrushes or sweeps as well as outward bursting of fluid in the near-wall-region). Donohue et al., on the other hand, analyzed motion pictures which showed that, for the one polymer concentration used, there was a marked change in the structure of the wall-region resulting in a decrease in the quantity and intensity of the spatially averaged burst rate of the low speed streaks and, therefore, an apparent change in the turbulence production process.

Whatever the model, the mechanism of drag reduction is dependent on many coupled and non-linear phenomena in the polymer-solvent system, thus complicating any testing procedure. It strongly depends on the polymer concentration in that not only the viscosity of the system increases but the probability of entanglements of polymer chains also increases with increasing concentration. There is even strong indication that drag reduction exists in the limit of infinite dilution (see Huang, 1974). The concentration of the higher molecular weight materials present in the molecular weight distribution influences, among other things, the degradation characteristics of a particular polymer flow. As Sylvester and Kumor (1973) note, the rate of degradation increases with polymer molecule size. Degradation can occur by both chemical and mechanical means, the analysis of which is complicated by the polymer-solvent system being used. Ignoring these effects could cause errors in the interpretation of experimental results. The dimensions of the flow apparatus

and the turbulent flow time are also factors to be considered as it is the shear field which controls the hydrodynamic forces on the polymer chains and therefore, the rate of degradation. The polymer and solvent mixing procedure is also extremely important. Careful and controlled methods for mixing and transferring batches of polymer solutions are essential.

There have been various conventional techniques used in making measurements in polymer flows, but most of the results have been inconclusive due probably to the effect of the additives upon the measuring instruments used, as shown by Freihe and Schwarz (1969) to be the case for hot films and Pitot tubes.

In the case of Pitot tubes, it is shown by Berman et al. (1973), for example, that the polymer terminal relaxation time, the fluid velocity and the Pitot tube diameter affect the measurements. Hot film anemometers, on the other hand, have different heat transfer characteristics in polymer solutions as compared to water and therefore cannot be calibrated using the usual heat transfer laws. They also suffer from a build-up of polymer on the film.

The successful techniques so far used for point measurements of the velocity have either been by flow visualization with dye or bubbles or by laser velocimeters. The flow visualization methods allow a good qualitative picture of the flow, but quantitative measurements are extremely difficult to obtain, as well as being very tedious and time-consuming. The results, at most, offer only a limited amount of the information normally of interest in turbulent studies. See, for example, Soyler and Metzner (1969).

Over the past ten years, since Yeh and Cummins (1964) demonstrated that fluid velocities could be measured by means of the Doppler shifted radiation of monochromatic light scattered off of particles in the fluid, the laser Doppler velocimeter (LDV) has been increasingly used for such measurements. In particular, it is ideally suited to polymer flow studies as it provides a direct measurement of the flow characteristics independent of the physical properties of the fluid. The light beams do not disturb the flow and it is only necessary that the fluid be transparent and contain a sufficient quantity of small flow-following scattering particles.

Application of the LDV to measurements in a polymer flow have been attempted. The works of Chung and Graebel (1969) and Guenterberg (1972) reported measurements of velocity profiles and axial turbulence intensities in a pipe flow. Kumor and Sylvester (1973) used an LDV system to study the effects of degradation of polymer solutions on the mean velocity and axial turbulence intensities in the turbulent boundary layer of a submerged flat plate in a water tunnel. Rudd (1972) measured both the mean axial profile and axial intensity across a square pipe with one polymer concentration.

The most difficult aspect of the LDV has been the processing of the signals obtained from the photodetector which detects the Doppler shifted frequency of the laser beam. Work on the development of processing systems has recently received a great deal of attention. In early measurements, a spectrum analyzer was used allowing the experimenter to obtain information on the mean Doppler frequency and mean square and higher order statistical correlations. This technique has, however, some limitations. A complete spectrum analysis of each data point is

necessary requiring long test runs. But more significant is that by operating in the frequency domain, the time history of the signal is lost, thus preventing the obtaining of instantaneous values, an area of particular interest when the simultaneous analysis of two or more velocity components is desired.

With the FM portion of the signal carrying all the information of interest, the wave analyzer has been supplanted by signal processing techniques in which the frequency signals are automatically followed by frequency trackers. Rapid developments in monolithic circuitry have had a strong effect on the ever-changing state of the art of laser velocimeter signal processing systems. Digital systems, using an arrangement of frequency counters, digital logic and digital computer, are being increasingly used. They offer better accuracy than frequency trackers in many applications. See, for example, the Proceedings of the Second International Workshop on Laser Velocimetry, edited by Stevenson and Thompson, (1974).

Assessing the present state of laser Doppler velocimetry, it is of particular significance to note the observations made by Durst et al. (1972). They note, for example, the extremely small number of reported measurements of fluid-dynamic significance made to date with an LDV system with which, exempting the work by Dunning and Berman (1973), not even satisfactory spectral measurements have been made. They remark that this undoubtedly stems, in part, from the multi-disciplinary nature of the subject, which requires a knowledge of optics, electronics, data processing and fluid dynamics. A review of the LDV literature bears this out where there are sometimes two or three authors for a paper each contributing his particular expertise. There is much to be said for a team

effort if some element of success is to be expected.

It is clear that an important step in getting reliable and significant data rests in knowing the capabilities and performance characteristics of the measuring system. Therefore, in the present work an attempt was made in evaluating the available LDV system in order to assess its reliability and accuracy.

With this evaluation, the LDV system was then used to extend the knowledge of turbulent drag reducing flows. There were two goals. First, polymer degradation in a low polymer concentration pipe flow with an in-line centrifugal pump was documented. This is not known to have previously been done. Secondly, mean velocity profile measurements were made of some of these flows with fresh, undegraded polymer. Particular interest was centered on the near-wall-region. This, as has been noted, is the region where the polymer-turbulence interaction is known to occur. While several studies have made velocity profile measurements this is the first time that a series of low concentration pipe flows have been studied using an LDV system. Details of these results are presented in Chapter V.

Basic information on the flow system used is presented in Chapter II. As the procedure for polymer preparation can affect the experimental results, a detailed description of the method employed is given together with an outline of the way the dissolved polymer was injected into the flow system. This is followed by a brief description of scattering particle considerations with some observations using different scattering elements.

In Chapter III a detailed critique of the optic system used is given. Although results have been published using this system (Guenterberg, 1972), it has never been analyzed. Discussion on signal-to-noise and broadening

are included since they are affected by the optical components and optical mode employed. The test volume size is calculated from transmitting and receiving optics considerations. Its dimensions specify the spatial and frequency resolution possible with the LDV system and determine the average number of particles in the test volume at any instant.

The crucial factor in extracting real time velocity information from the photodetector lies in the capabilities of the electronic processing equipment. The present experiments were carried out with a phase-locked loop frequency tracker originally built by Electronics. Due to constant breakdown of some components as well as having the original goal of taking two-component data with two, identically performing units, much time and effort was spent in matching components of two originally mismatched and failure-prone units. This endeavor has resulted in only one unit functioning to fair satisfaction. Chapter IV describes in detail this frequency tracker. A critical analysis of its ability to give accurate velocity information is also presented. Neither a detailed description nor an analysis of this frequency tracker's capabilities had previously been attempted.

CHAPTER II

THE FLOW SYSTEM

General Description

The general layout of the closed-loop flow system used is illustrated in Figure 2.1. City water enters the system as indicated in the figure, allowing the system to be filled to a capacity of approximately 2385 liters. The large, glass-lined, tank contains some 90% of the storage capacity. The approximately 39.6 meters of 5.08 cm I.D. piping is polyvinyl chloride (PVC) pipe with the exception of the vertical length between the mixing tank (small tank) and the test section which is made of brass. Thus, oxidation of the inner linings of the flow system and contamination of the fluid is kept to a minimum.

The system, once filled, and with the appropriate valves closed, is driven by an American Marsh centrifugal pump rated at 567 liters/minute (30.5 meter head, 1750 rpm) and powered by a General Electric 220/440 Volt, 7 1/2 HP A-C motor. For a test condition of approximately 50,000 Reynolds number in the test section, this implies a relatively low utilization factor for the pump, thus causing some concern for the possible polymer degradation effects. This will be discussed in a later section.

The flow rate is monitored by a Potter turbine flow meter upstream of the test section, whose signal is amplified and counted on a digital counter. Large velocity adjustments can be made by opening or closing the globe valve upstream of the test section while finer adjustments are made by means of an electric motor with a remote control built into the

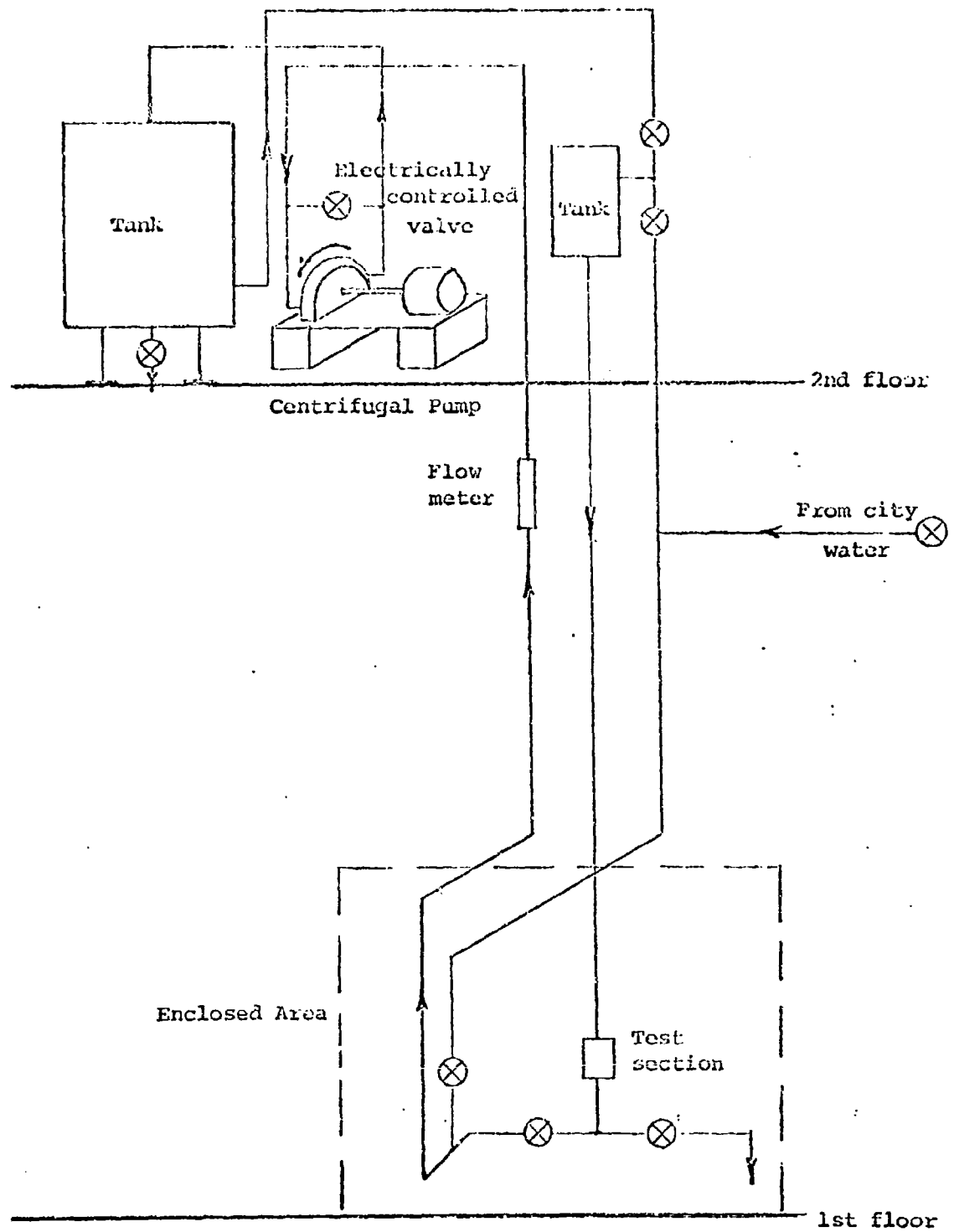


FIGURE 2.1

FLOW SYSTEM

pump bypass valve. For a Reynolds number of 50,000, it takes an average of approximately 20 minutes for the fluid to make one complete pass through the system. Reynolds numbers of at least 100,000 are possible.

The pressure drop is measured by an ITT Barton 0-0.105 kg/cm² differential pressure cell with a dial indicator. Instantaneous readings are obtained through a potentiometer built into the dial indicator. Sidewall pressure taps some 362 cm apart are located below the small settling tank and upstream of the test section. The first pressure tap is some 51 diameters below the tank exit.

The small, epoxy-lined tank, just upstream of the test section, serves in straightening out the flow as it contains a 15.2 cm high, 1.27 cm diameter honeycomb mesh. A fresh concentration of polymer solution is injected through the top of the tank so it also serves as a mixing reservoir for the water and polymer. The fluid passes through approximately 6.1 meters of straight 5.08 cm diameter smooth pipe before entering the Plexiglas test section ensuring that the flow is well-defined and that effects due to entrance, turns, etc. are negligible.

A Weiss angle-stem thermometer was inserted into the wall of the PVC pipe some 270 cm downstream of the test section. Continual monitoring of the flow temperature was necessary since the kinematic viscosity is quite sensitive to temperature. The centrifugal pump gradually heated the water.

Polymer Preparation and Injection

The polymer powder used during these experiments (January - April, 1974) was Separan AP-30 (dated June, 1973) a polyacrylamide manufactured by Dow Chemical Company with an average molecular weight of $(2-3) \times 10^6$. It is a good drag reducing agent and is less susceptible to shear

degradation than polyethylenes like POLYOX WSR-301, as shown, for example, by Ellis and Ting (1972).

As it takes a considerable amount of time for the polymer to completely dissolve in water (Chung and Graebel, 1969), master batches of completely dissolved but large concentrations of polymer were prepared. The master batch was then slightly diluted, to allow it to be pumped easily into the flow system through a 10 mm circular opening at the top of the small tank, utilizing a variable speed, Masterflex tubing pump. As mentioned in the previous section, the tank serves as a mixing reservoir for the injected polymer solution and the flowing water, with the tubing pump speed adjusted to allow continuous, even mixing of the polymer solution in the flow system.

Velocity profiles were obtained by injecting polymer concentrations of 10, 20, and 40 ppm (parts per million by weight). Larger concentrations were attempted but it was found that it was not possible to dissolve them in the flow before arrival at the test section. The design of the flow system did not permit any alternate mixing procedures to be attempted without additional risk of mechanical degradation of the polymer. Larger concentrations were used, however, for the degradation studies.

Relatively elementary techniques were used in the master batch preparation. Since the polymer is hygroscopic, small quantities (approximately 50 ml), at a time, of methanol, a non-solvent of Separan AP-30, were placed in a beaker and some 10 grams of Separan AP-30 added to it. While continuously agitating the beaker containing this slurry, small amounts of it were gradually, but continuously, dispersed on the surface of a large surface area beaker containing approximately a liter of

distilled water. This second beaker, in turn, was continuously but slowly stirred with a thin rod thus preventing to a significant degree clumping of the polymer upon contact with the water, as well as enhancing the dispersion and dissolving of the powder. The process was continued with fresh distilled water and additional slurry until the prescribed quantity of polymer for a 10, 20, 40 etc. ppm run was completely dissolved. It was possible, for example, to get a 40 ppm quantity of polymer (96 grams) dissolved into 30 liters of methanol and water solution, implying a batch concentration around 3200 ppm. It was found that in allowing this batch to sit for less than a day, the polymer not only became completely dissolved but the small air bubbles that were put into solution during the mixing process gradually came out of solution.

As city water was used in the flow system, there was a possible degradation effect of the chlorination on small concentrations of polymer. Thus, 18 grams of sodium thiosulfate ($\text{Na}_2\text{S}_2\text{O}_3$) were dissolved and routinely added to the flow system as a dechlorinator several hours before running tests.

Scattering Particle Considerations

The influence of the scattering particles on the quality of signal obtained from the laser velocimeter is extremely important. The signal contains both amplitude and frequency modulation as well as wide band noise but the only information of interest is the FM component. The depth of this modulation is influenced by the scattering particle size and concentration as well as the beam alignment and the relative beam intensities. But, as Durst et al. (1972) indicate, there is little published information relating specifically to the presence of particles in the fluid.

In the present experiments it was observed by looking at the quality of the modulated and demodulated Doppler signal on an oscilloscope, that the water naturally contained an ample concentration of suspended particles (also observed to be the case by Durst et al. 1972, among others). The addition of milk and Styrene/Butadiene latex particles was tried as additional scattering agents in order to determine whether they improved the modulated and demodulated signals obtained from the naturally seeded water. A $5 \cdot 10^7$ particles/cm³ (average particle size of 0.3 μ m) concentration of homogenized milk, suggested by George and Lumley (1973) as providing an excellent signal-to-noise ratio, was used. Despite the high scattering qualities observed, the presence of the milk produced no noticeable changes in the signals. Similar to Guenterberg (1972), a concentration of $2 \cdot 10^{-3}\%$ (average particle size of 0.1985 μ m) of latex particles was also used. Again, no observable differences in the modulated and demodulated signals were noted. This observation decided against its use (also, it might be noted that the latex has a prohibitively high commercial cost and to make it from raw styrene is a sensitive procedure).

In a recent report by Keller et al. (1974) the nucleus spectrum (particle and bubble content) of the water that was used in the present experiments was presented. The technique used in measuring these nuclei utilized the optical behavior of the nuclei for their recording. It was limited to sensing nuclei of 6 μ m diameter and above, due to electronic limitations present in the recording system. More recent and as yet unpublished data for the untreated tap water has allowed, however, extrapolation down to 1 μ m resulting in a minimum possible number of nuclei of 104,922 particles/cm³ ranging from 1-10 μ m in diameter. As

noted in the chapter on the optical system, the results indicate the existence of sufficient scattering elements in spite of the size measuring limitations. As there is a most probably higher concentration of even smaller scattering particles, these must be included in the total concentration which is responsible for the observed Doppler signal quality.

CHAPTER III

THE OPTICAL SYSTEM

Description of Optical System

The optical layout used was of the 'reference beam' or 'local oscillator heterodyning' mode originally employed by Yeh and Cummins (1964) and subsequently by numerous investigators. In this configuration, (Figure 3.1), the reference beam is directed onto a photocathode, in this case a photomultiplier, where it beats with light scattered from a stronger beam (called the incident beam) by particles assumed moving with the flow. The light scattered from the natural contaminants in the water is Doppler shifted by an amount $f_D(t)$ so that the beating on the photocathode takes place between the reference beam frequency, f_0 , and the frequency of the scattered light $f_s(t) = f_0(t) + f_D(t)$, resulting in a photomultiplier output voltage whose frequency is the instantaneous Doppler frequency.

The equation relating the measured frequency shift in radiation, $f_D(t)$, to the instantaneous velocity $\underline{V}(t)$ can be derived by considering the Doppler shift of scattered light that occurs. The equation takes the form

$$f_D(t) = \frac{2}{\lambda} V(t) \sin \frac{\phi}{2} \quad (3.1)$$

where λ is the wavelength of the laser light in air, ϕ is the angle between the reference and incident beams, i.e. the scattering angle, and $\underline{V}(t)$ is the particle velocity in the direction perpendicular to the bisector of the reference and incident beams.

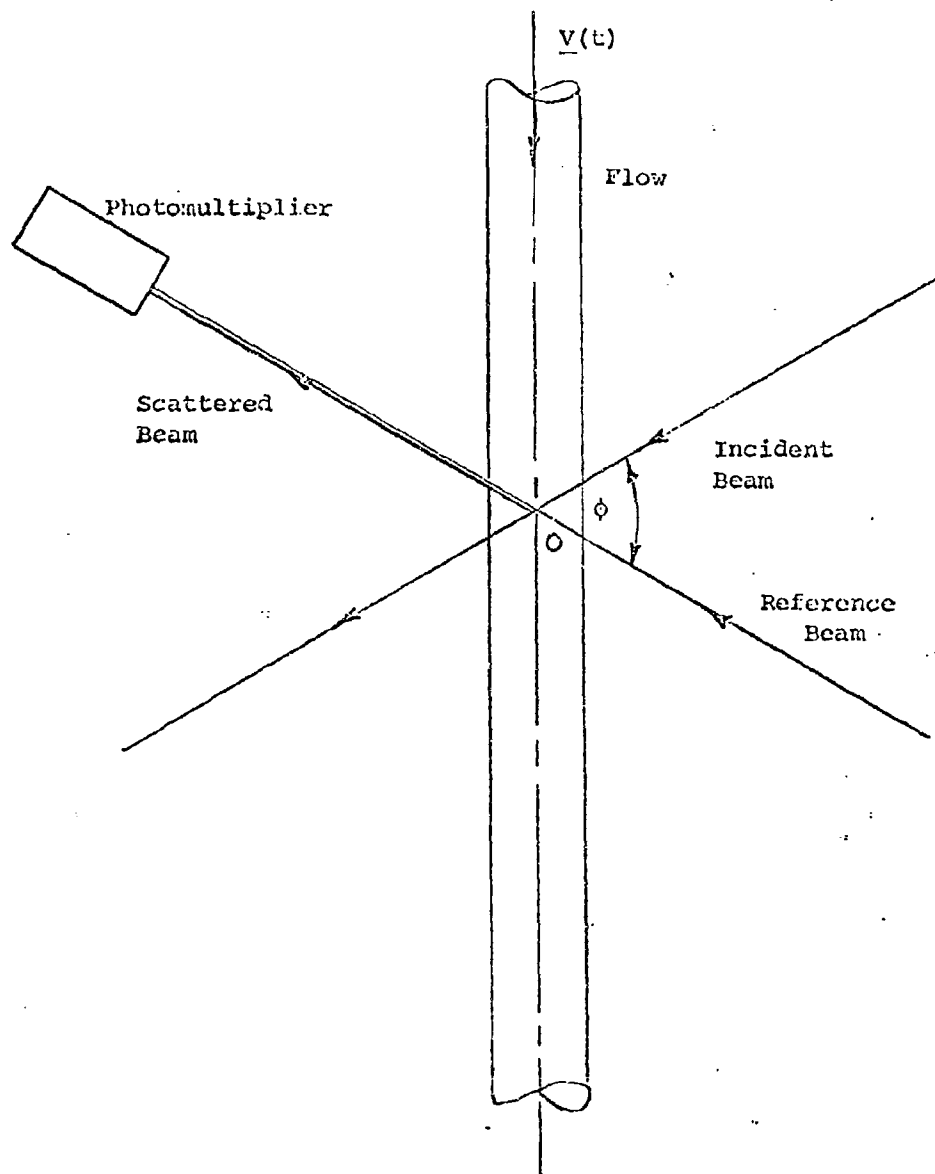


FIGURE 3.1

TYPICAL REFERENCE BEAM SYSTEM

An alternate and yet perfectly equivalent way of describing the heterodyning effect might be easier to understand (see Rudd, 1969). The two beams (incident and reference) intersecting at point 0 in Figure 3.1 could be thought of as forming a set of virtual fringes where they overlap. As a particle crosses these fringes it blocks off a varying amount of light and it is the variation in intensity of this transmitted light that is observed on the photomultiplier.

This fringe model is normally used to describe the other widely used optical arrangement originally proposed by Rudd (1969) and known as the dual-scatter mode. In this mode (see Figure 3.2) two incident beams, of equal intensity, are made to intersect and produce a real fringe system as a test volume. There is no reference beam. Instead, scattered light from particles crossing the fringes causes, as in the fringe description of the reference beam mode, a rise and fall of the light intensity arriving at the photodetector at a rate (Doppler frequency) proportional to the velocity at the test point. A discussion of the relative merits of the two optical modes in their application to the present experimental effort will be given in the section on signal-to-noise and broadening.

As noted by Jackson and Paul (1971), the laser anemometer offers, in contrast to a hot wire anemometer, a linear response between the velocity and the Doppler frequency measured. It requires no calibration due to the absolute characteristics of the variables in equation (3.1) for a given fluid medium.

In the experiments described here, a two-component optical geometry was employed as illustrated in Figure 3.3. The coherent light source was a 5 mW Spectra Physics helium-neon laser of 6328Å. Beam splitters BS₁ (10% reflection) and BS₂ (25% reflection) mounted at 45° to the horizontal,

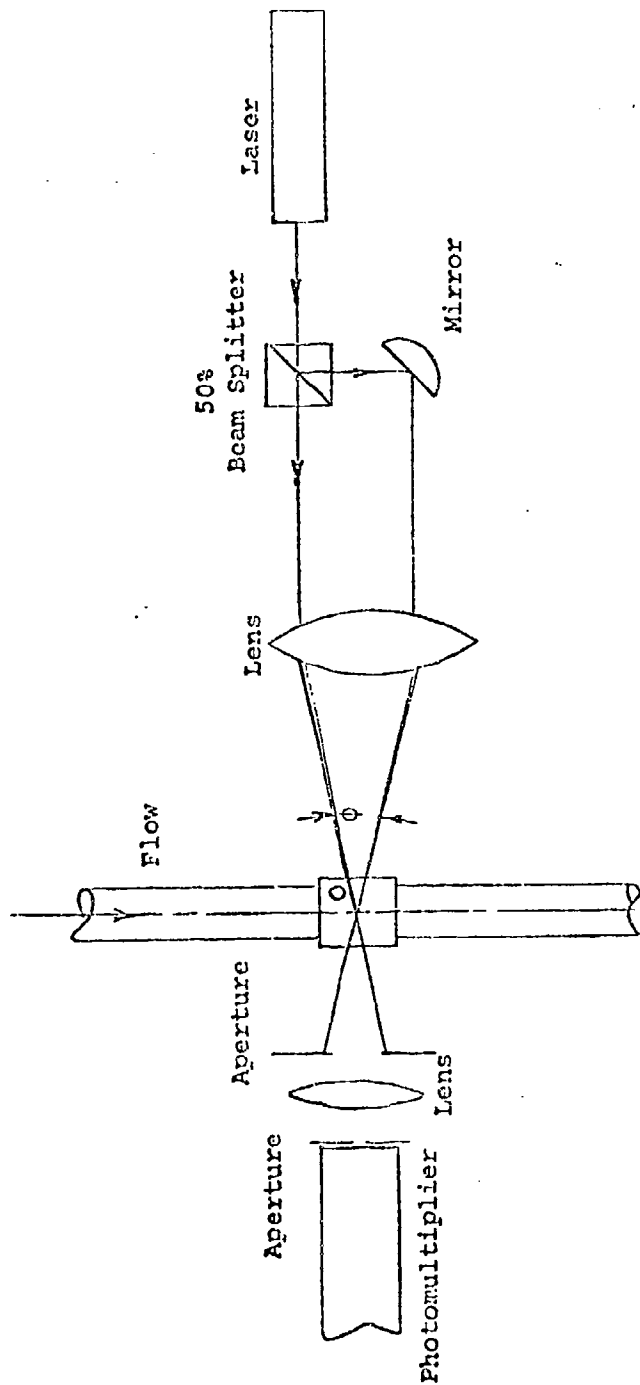


FIGURE 3.2

TYPICAL DUAL-SCATTER SYSTEM

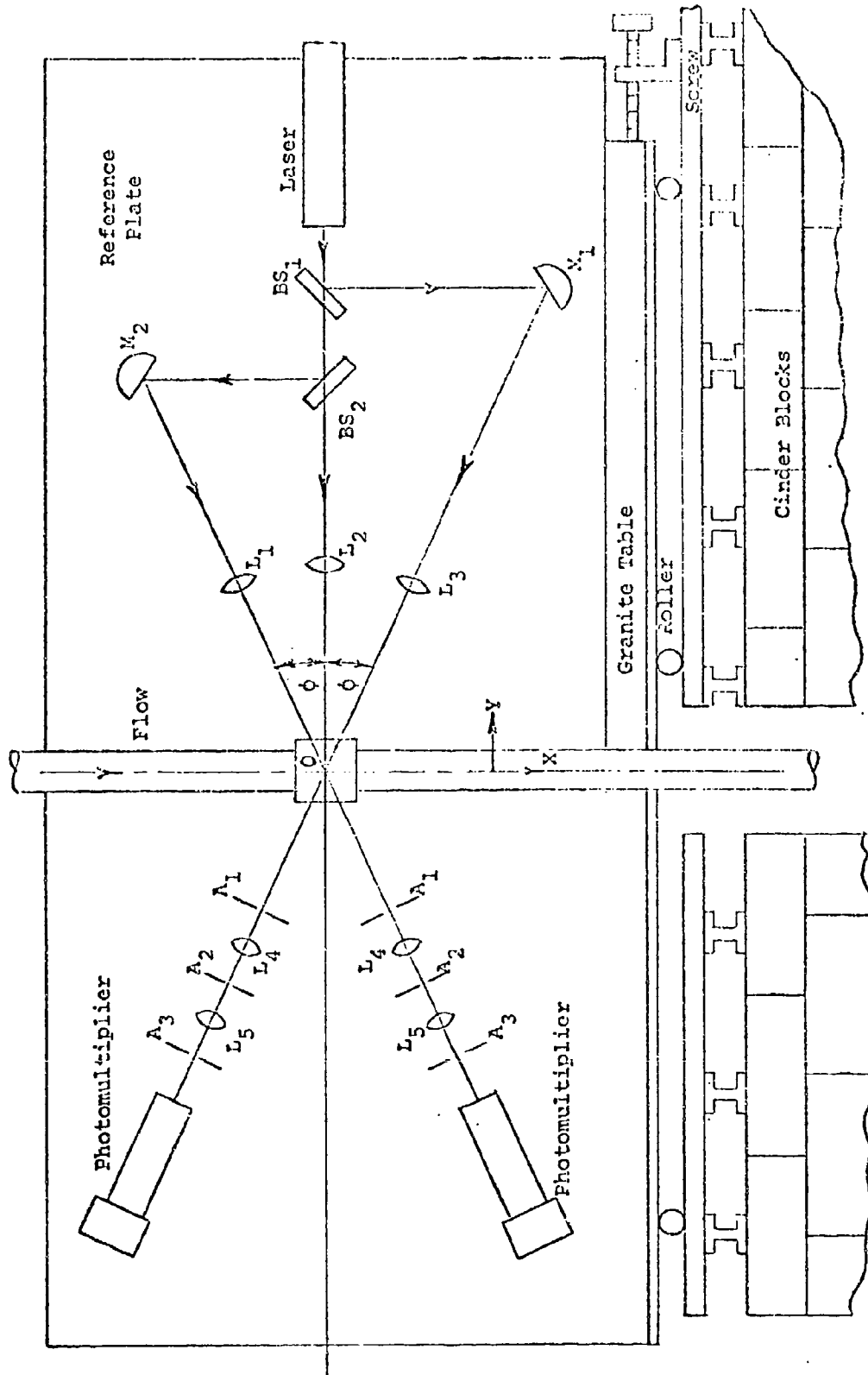


FIGURE 3.3
TWO-COMPONENT OPTICAL GEOMETRY

serve in splitting the 1.5 mm diameter laser beam into two reference beams and an incident beam. Magnetically mounted mirrors M_1 and M_2 can be adjusted to allow the three beams to intersect in a vertical plane at a point 0 within the test section. The angle between the incident beam and each one of the reference beams was adjusted to $10^\circ 40'$ within an error of $20'$ of a degree. This was the same margin of error obtained in aligning the three beams in a vertical plane through their respective lenses and then through the centerline of the 2" I.D. Plexiglas test section (index of refraction 1.5). The transmitting lenses L_1 , L_2 , and L_3 (16 mm DIA, 124 mm focal length, achromatic) are mounted and aligned to focus on the test point. The intersection of each of the reference beams with the incident beam forms what is known as the measuring or test volume for that particular reference beam. Under proper alignment, this intersection is assumed to form approximately the same volume in space for each of the reference beams. The resulting optical geometry provides a method for obtaining the axial and radial components of velocity. A one component setup can be obtained by replacing ES_2 with a mirror.

To obtain measurements across the test section, point 0, the test point, was moved relative to the test section. This was done by turning the spring-loaded screw shown in Figure 3.3. This caused the entire optical system, and therefore the test point, to be moved as a unit since all optical components, with the exception of the test section, were rigidly mounted on the reference plate which in turn was fastened to the granite table. After accurate angular and vertical alignment of the beams through the centerline of the test section, translations of the granite table (and therefore the test point) could be determined within .025 mm by a dial indicator mounted at the end of the table.

Figure 3.4 indicates the layout of the optical receiver for one of the two identical channels. After passing through point 0, the reference beam must pass through a pair of apertures and lenses and a pinhole before striking the photocathode surface.

This is a crucial optical alignment. As indicated by Mazumder and Wankum (1970) and George and Limley (1972), the instrumental broadening (frequency spread) of the signal arriving at the photocathode is directly related to the area of the optical receiver. This will be discussed in the section on signal-to-noise and broadening.

The pinhole-lens combination was designed with the intention of projecting a real, inverted image of the test point, 0, on the photomultiplier tube. The portion of the reference beam which does not intersect the scattered radiation, from the test point, onto the photocathode surface, induces shot noise without an increase in signal strength. The pinhole was placed at the focal distance of the two receiving lenses for the purpose of blocking the unwanted portion of the reference beam (the portion with amplitude less than $1/e^2$ of its peak intensity is usually considered "unwanted") as well as any stray light from particles outside the test volume. This allows only the small portion of Doppler scattered radiation, colinear with the remaining part of the reference beam, to pass to the rear lens and to be then focused on the photomultiplier.

Use of the rear lens in focusing the beam to a life size image of the test volume diameter has no apparent advantages. There appear to be, however, some disadvantages. There is a signal intensity loss of approximately 4% for each of the two lens surfaces as well as the additional potential problem of flare caused by the lens.

The front adjustable aperture was useful in aligning the instrument

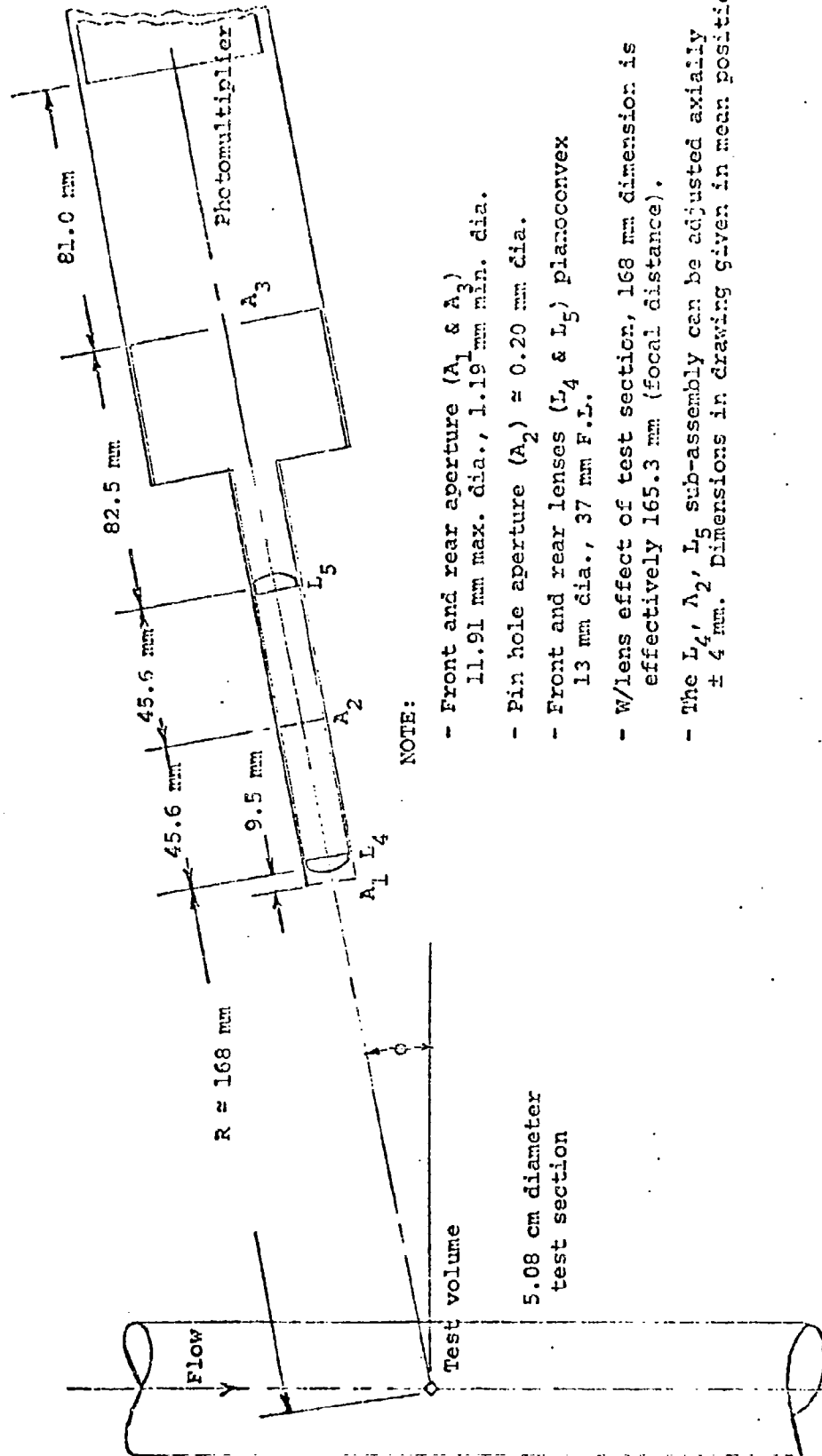


FIGURE 3.4

RECEIVING OPTICS LAYOUT

and prevented some of the unwanted light from extraneous sources from entering the receiving optics housing. It was maintained in its maximum diameter position of 11.9 mm in order to minimize broadening of the light beam arriving at the pinhole. The rear aperture served no apparent purpose and was left in an open position. An improvement on the receiving optics design might include removal of the rear lens and aperture.

All the receiving optics components were arranged into a semi-integrated package by being placed into a light-sealed, rigid housing in which relative locations of individual components remained fixed. The fine alignment and focusing of all beams onto the test volume and then through the receiving optics housing was not, however, the easiest due to the individual adjustments that had to be made on the transmitting lenses and beam splitters before aligning the beams through the optical receiver housing. There is much to be said for an integrated optical system (see for example Durst and Whitelaw, 1973) which provides the possibility of accurate alignment in at least one optical mode with a minimum of adjustments. This also assures a minimum of signal broadening due to possible misalignments.

All internal surfaces of the receiving optics were chemically blackened to minimize any possible incidence of stray light. All reflecting surfaces of the optical bench were painted with ultra-flat black.

A detailed description of the mounting of the optical components can be found in Guenterberg (1972).

Test Volume Size

The test volume is the region from which the Doppler radiation information originates. A look at the volume size and its implications is therefore a necessity since its dimensions specify the spatial resolution

characteristics of the particular velocimeter system being used.

As George (1972) quite clearly points out, the LDV responds to a particle averaged velocity and not the Eulerian velocity that might be measured by a fixed probe like a hot wire. This implies that in order for the average particle velocity to be interpreted as the average Eulerian velocity over the test volume, there must be a length criterion such that the time a particle spends in the test volume is short compared to the evolution time of the turbulence. Therefore, the largest dimension of the test volume must be much smaller than the scale of turbulence inhomogeneity. This is also the case in considering velocity fluctuations.

The size of this volume depends on both the transmitting and receiving optics. Formally, it can be defined as the region in space within which the Doppler signal amplitude is at least $\exp(-2) = 0.135$ of its peak value, where the peak signal amplitude occurs as a scattering particle passes through the geometrical center of the crossover region formed by the transmitting optics (Brayton and Goethert, 1971). But this defined volume is not necessarily the effective scattering region because the receiving optics may not be looking at the same volume. Further analysis must be considered.

If the intersection of the two reference beams is considered to form the test volume, with the scattering beam aligned in its appropriate position, the volume, approximated by an ellipsoid, can be calculated by the formula (Mazumder et al., 1972),

$$V = \frac{2}{3} (D_T)^3 \cdot \left[\frac{1}{\sin 2\phi} + \frac{1}{2 \tan 2\phi} \right] \quad (3.2)$$

where D_T is the Airy disk diameter of one of the three transmitting lenses of focal length f_1 ,

$$D_T = \frac{2.44 \cdot \lambda f_1}{a} \quad (3.3)$$

and where a is the diameter of the transmitting aperture which in the present case is taken to be the exp (-2) beam intensity diameter of the monochromatic, coherent light of the laser and λ is its wavelength. Calculation shows that the test volume defined by the transmitting optics is 0.0051 mm^3 .

The effective scattering region of this test volume is the portion of the above defined volume intersected by the field of the receiving optics. The effective diameter of this region has an upper limit specified by the transmitting optics and a lower limit set by the diffraction limit of the receiving optics.

In order to make this effective volume as small as possible, the imaging optics should have a minimum of spherical aberrations. This is clearly the case when using plano-convex lenses for the receiving optics where the convex surface is facing the incident radiation. With a minimum of the optical surface of these lenses being used (in the present case specified by the front receiving aperture diameter), it can be shown, using third order theory (Jenkins and White, 1957), that the image defects are at a minimum. In fact, for the existing optics, calculations indicate a lateral spherical aberration of $0.83 \text{ } \mu\text{m}$.

Considering diffraction limited optics in assessing the resolving power of the receiving optics, Airy's disk formula, equation (3.3) was used with f as the focal length of one of the receiving lenses and a the effective diameter of the lens, which in this case is closely approximated by the minimum aperture opening. This gave a disk diameter of $48 \text{ } \mu\text{m}$ and therefore the lower limit to the effective volume diameter.

This is, therefore, the smallest length that can be resolved in the mean flow direction.

With a magnification of the test volume on the image plane of the pinhole of approximately 0.28, this would indicate that for a disk diameter of the test volume (specified by the transmitting optics) of approximately 0.124 mm, the pinhole aperture would have to be no more than 0.034 mm in diameter. As the pinhole is approximately 0.20 mm in diameter, the effective test volume diameter seen by the photomultiplier is no less than that defined by the transmitting optics, namely, 0.124 mm. This implies that some unwanted light originating outside the test volume diameter is allowed to pass through to the photomultiplier resulting in a decrease in signal-to-noise. The pinhole with its present location and size acts as no more than a baffle to unwanted light outside this 'enlarged' test volume.

Assuming diffraction limited optics, the effective length ΔY of the test volume in the radial direction of the pipe (see for example, Brayton et al., 1972) is approximated by the formula,

$$\Delta Y = \frac{4\lambda}{\pi \Delta\phi \sin \phi}$$

where $\Delta\phi$ is the angle of convergence of the incident beam focused by the transmitting lenses and ϕ , as before, is the angle subtended by the reference and incident beams. This gives a radial dimension for the effective test volume of 0.69 mm which is not influenced by the receiving optics.

With the effective test volume known, an estimate of the number of scattering particles in the test volume at any time could be made. Table 3.1 shows the results. As was noted in the section on scattering particle considerations, the results of Keller et al. (1974) and more re-

TABLE 3.1

PROPERTIES OF SCATTERED PARTICLES USED

Scattering Element	Average Size μm diameter	Concentration in flow (per cm^3)	No. of Particles in Test Volume
Latex	0.1985	$6.1 \cdot 10^9$	31,341
Milk	0.30	$5 \cdot 10^7$	257
Water*	5	$10.5 \cdot 10^4$	0.539

* Data available extrapolated down to 1 μm .

cent unpublished data were limited to measurements of scattering elements of 5 μm in diameter and above. By extrapolation, this can be extended down to 1 μm . Naturally, there are smaller bubbles and particles in the water with a most probably higher concentration than those within the range measured. A rough calculation can show that this distribution of smaller scattering elements would not result in more than approximately one element in the test volume at a time resulting in sufficient Rayleigh scattering to warrant not adding any new particles.

Of particular importance to the electronic processing system, and therefore the experimental results, is the frequency resolution possible with the optical configuration used. The frequency window of the test volume can be determined with knowledge of the dimensions of the pipe and test volume. For example, with the characteristic mean velocity $\bar{V}(t)$ at the centerline of the pipe of 1 m/sec and with a pipe diameter of 5.08 cm and a test volume characteristic length of 0.69 mm, the frequency window can be estimated to be between 20 and 1450 Hz where $f = \frac{\bar{V}(t)}{L}$, L being the length scale. Further reference to the frequency resolution will be made in the following sections.

Signal-to-Noise and Broadening Considerations

The two most important parameters governing the sensitivity of an instrument are its signal-to-noise ratio and its frequency response. With the LDV instrument package, the sensitivity of the electro-optical components offers a good indication as to the requirements placed on the electronic system which, with some degree of accuracy, is to process the transmitted signals.

Since from equation (3.1) the wavevectors are determined by the wavelength of the radiation and the geometry of the flow-measuring instru-

ment, measurement of the frequency shift should, in theory, lead to a precise measurement of the fluid velocity. However, in practice, there are a number of effects which cause the signal to be broadened. This is also referred to in the literature as Doppler ambiguity, an analysis of which will give some estimates as to the spatial resolution of the system.

The principle ambiguity is a result of the finite residence time of the scattering particles in the test volume. The arrival of the scattering particles at arbitrary times gives rise to random fluctuations in the phase of the Doppler signal. As Edwards et al. (1971) demonstrate, this is equivalent to the degree of uncertainty in the incident and scattered vectors as determined from optical considerations. This results in a broadening of the frequency spectra.

An estimate of transit time broadening in the present optical configuration can be made assuming for the moment, axial, laminar flow while looking at just the optical receiver. Differentiation of equation (3.1) gives

$$\frac{\partial f_D(t)}{\partial \phi} = \frac{2}{\lambda} V(t) \cos \phi. \quad (3.4)$$

Now, referring to Figure 3.4, if R is the distance from the front aperture of the optical receiver to the measuring point (taken at the centerline of the pipe) and if r is taken as the minimum front aperture radius, the incremental angular uncertainty, $\Delta \phi$, can be written as

$$\Delta \phi = \frac{2r}{R}.$$

The transit time broadening due to the finite aperture in the light collecting system is, therefore,

$$\Delta f_a = \frac{\partial f_D}{\partial \phi} \Delta \phi = \frac{4r}{\lambda R} V(t) \cos \phi. \quad (3.5)$$

This gives an ambiguity of approximately 23.7 KHZ. For a typical mean Doppler frequency of 300 KHZ at a Reynolds number of 50,000, this means that there is an estimated 8% broadening in the mean Doppler signal received by the processing circuit. The 20 minutes of a degree misalignment in the incident and reference beams is of negligible importance.

Broadening can also arise from the velocity gradients within the measuring volume, from turbulence intensity broadening, the Gaussian intensity distribution across a laser beam, the signal processing equipment, as well as from other normally minor sources. These have not been estimated for the present system and are more readily obtained and analyzed by spectrum analysis of some real signals (see, for example, Roberts, 1974 and George, 1974). Where they cannot be eliminated from the signal they must be corrected for in the processing circuit.

It is clear from the above analysis of transit time broadening that in order to avoid frequency ambiguity it is necessary that scattered light be received from an extremely small solid angle. In the dual-scatter mode, there is no such limiting requirement. As seen in Figure 3.2, the scattered radiation from the flow particles directly generates the desired, heterodyned signal. The difference frequency can be shown to be the same at all points in the scattered lobe and is independent of the scattering angle or the spatial resolution and area of the receiving aperture. This implies that there is no signal broadening due to the receiving aperture. There is, as in the reference beam mode, transmission aperture broadening but Mazumder and Wankum (1970) demonstrate that for the dual-scatter mode it is quite small as well as being independent of the receiving aperture diameter.

Since the Doppler frequency is independent of the viewing angle in

the dual-scatter mode, another significant advantage of the dual-scatter configuration is that more scattered light can be focused on the photocathode than is possible with the reference beam mode. Therefore, the signal-to-noise ratio (S/N) is greatly enhanced. Drain (1972) and Mazumder and Wankun (1970) have calculated S/N as a function of detector aperture for both optical modes. A figure by Drain (1972), reproduced in Figure 3.5 is particularly informative.

In this figure it is assumed that noise arises only from the photodetector surface. A relative signal-to-noise ratio (assuming the mean scattering power of the fluid is constant) is plotted versus the coherence factor σ (aperture radius/coherence radius), where N_e is the mean number of particles present at one time in the test volume and where the coherence radius is approximated by the dimension of the test volume in the flow direction. For the reference beam mode it is seen, for example, that if N_e is assumed to be large, the S/N ratio approaches a limiting value of approximately twice that of the dual-scatter mode. The S/N depends on the amount of light scattered and not on N_e , but as has already been discussed and is not obvious from this curve, frequency broadening is not independent of the aperture.

In the present reference beam configuration the coherence factor for the minimum receiving aperture possible is approximately 3.0. From the calculated number of scattering elements in the test volume (≈ 1) it is quite clear, looking at Figure 3.5, that the dual-scatter mode will offer an increase in S/N. This result, combined with broadening considerations, indicates that the dual-scatter mode is more appropriate for the present application.

Despite the possible advantages to modifying the present optic

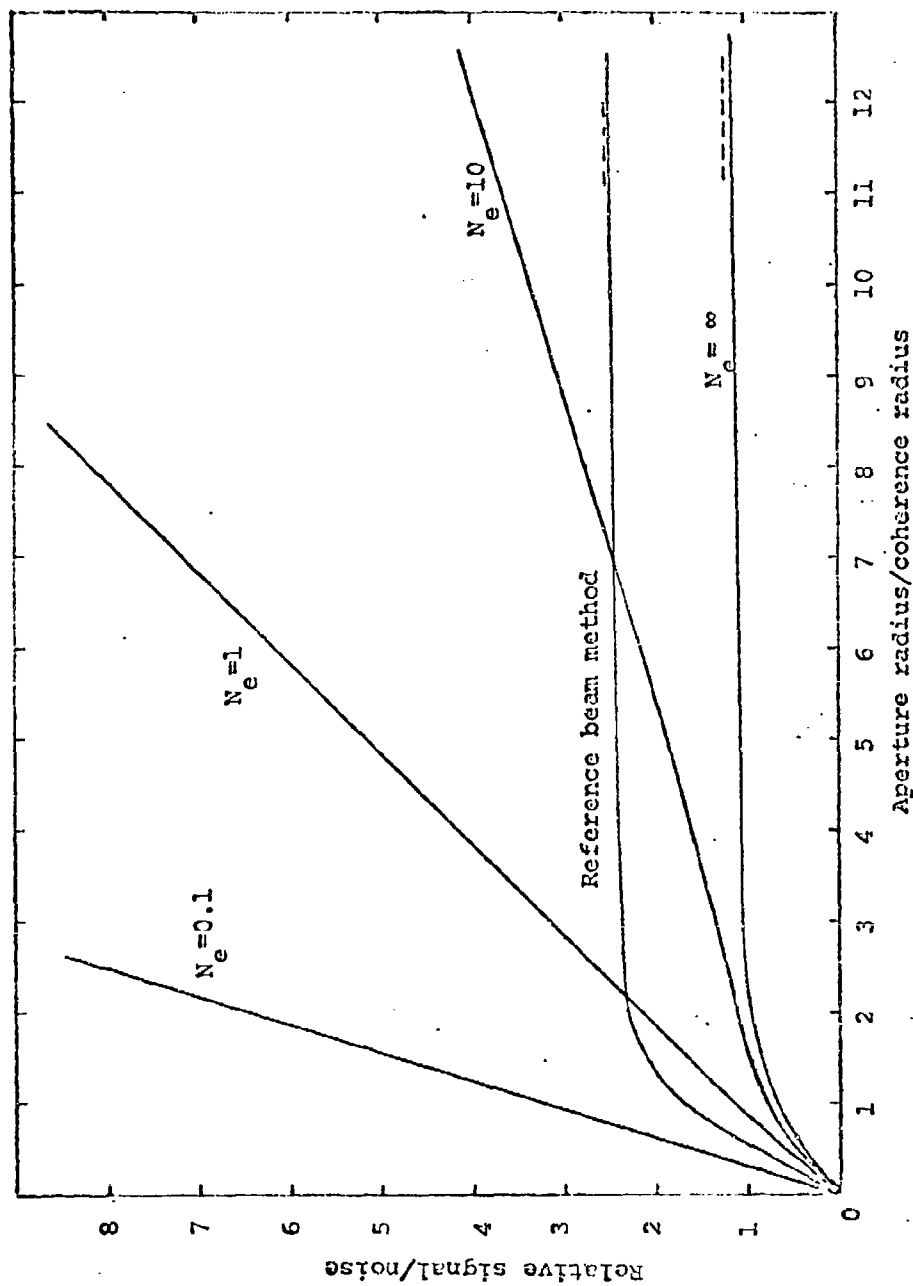


FIGURE 3.5

DEPENDENCE OF S/N ON DETECTOR APERTURE AND EFFECTIVE NUMBER OF PARTICLES FOR
THE DUAL-SCATTER AND REFERENCE BEAM MODES

system as implied by the above analysis and despite the suggested changes in the frequency tracker (see Chapter V), the present LDV system was shown repeatedly to be able to perform well in determining mean velocity profiles. This was shown to be the case by checking the centerline velocity readings obtained with the LDV with those obtained by flow meter readings and calculations using pressure drop measurements. Results from all three methods showed velocity agreement within 3.4% for fresh water. Therefore, the existing LDV was used for mean velocity profiles.

It will be shown in the following chapter, however, that the present LDV system is not capable of accurately determining turbulence intensities. It is recommended that, in addition to the suggested frequency tracker modifications to be made, an optic system similar to that outlined in Figure 3.2 be employed. This will provide a simpler and more accurate way of transmitting receiving optical signals. It includes an integrated transmitting optics package, available commercially, that is capable of being adjusted for either dual-scatter or reference beam operation with one internal adjustment. The receiving optics package would include, as in the present design, a front aperture and front lens and a pinhole more closely matching the test volume radius.

CHAPTER IV

THE SIGNAL PROCESSING SYSTEM

The laser Doppler velocimeter is a measurement system with three distinct components: 1) the laser and transmitting optics; 2) the electro-optical receiving elements; and 3) the signal processing electronics. The first two components were described and an assessment of their performance attempted in Chapter III. The remaining component will be described in this chapter.

The Frequency Tracker

A block diagram of the signal processing system is shown in Figure 4.1. It illustrates the path the signal must take from the photomultiplier to the final stage where voltages proportional to mean velocities and turbulence intensities across the profile are obtained.

The instantaneous velocity in the time domain, of any point in the fluid, can be described by a decomposition into a mean flow $\bar{V}(t)$ and a fluctuating component $V'(t)$,

$$V(t) = \bar{V}(t) + V'(t) . \quad (4.1)$$

The conversion of this time dependent velocity to a time dependent FM signal at the terminals of the photocathode results in a frequency fluctuation described by

$$f_D(t) = \bar{f}(t) + f'(t) \quad (4.2)$$

where $f_D(t)$ is the instantaneous Doppler frequency described in equa-

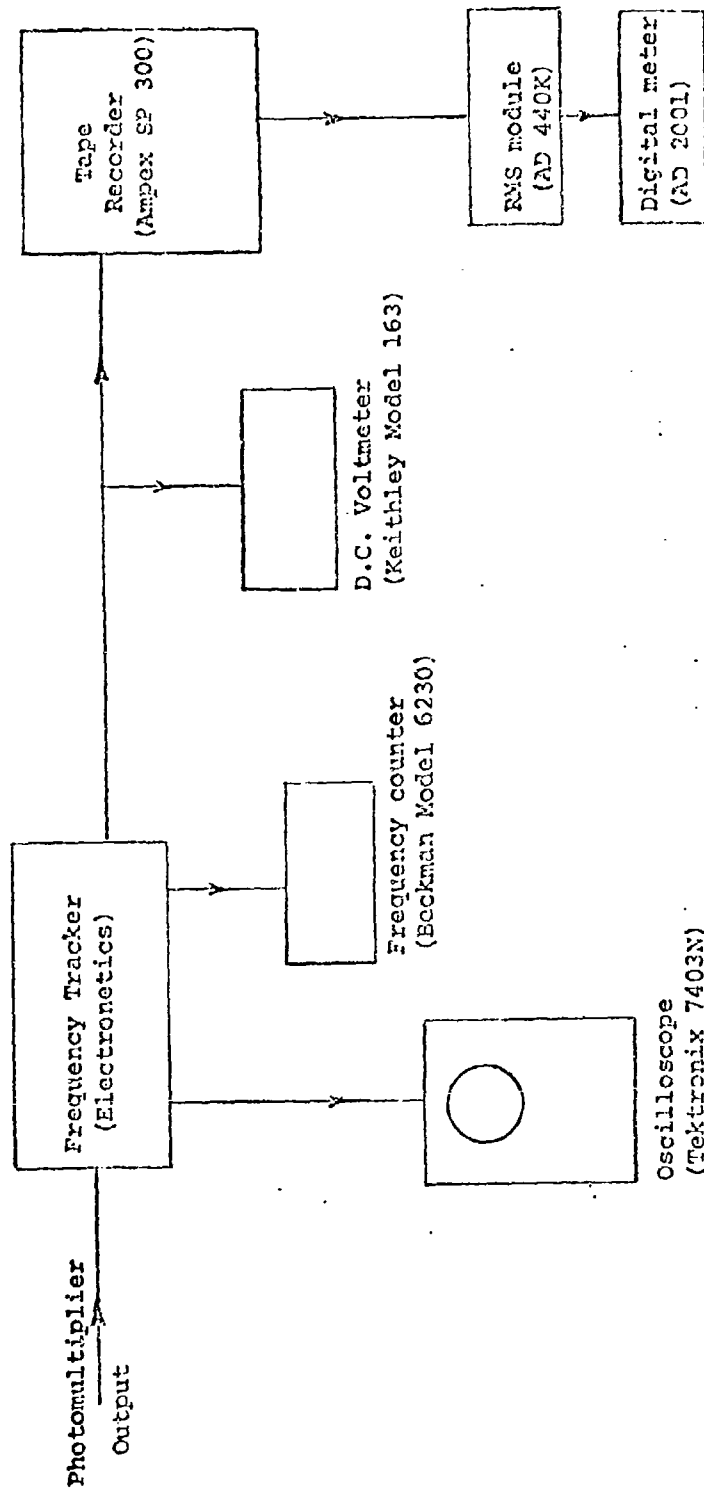


FIGURE 4.1

SIGNAL PROCESSING ARRANGEMENT

tion (3.1), $\bar{f}(t)$ is the carrier frequency corresponding to the mean velocity $\bar{v}(t)$ and $f'(t)$ is the frequency fluctuation corresponding to the velocity deviations $v'(t)$. Changes in the instantaneous velocity, therefore, result in a frequency modulation of the carrier frequency out of the photocathode at a rate proportional to the rate of velocity fluctuations.

The important factor in extracting real time velocity information from the photodetector lies in the electronic signal processing system. In order to obtain the mean velocities, turbulence intensities and the higher order distributions with precision it is essential that the Doppler signals be accurately demodulated. This implies a precise display of the carrier frequency, the frequency deviation, and the modulation frequency of the FM process. It requires that the frequency tracker that is used must be able to respond to the rate of change of velocity fluctuations of the turbulence intensities generated by the flow conditions, passing on the FM information while at the same time rejecting the noise in the signal bandwidth. The nature of the signals obtained in a turbulent flow is dependent on the type of velocimeter used in solving this complex signal processing problem.

A simplified block diagram of the frequency tracker used in the present experiments is shown in Figure 4.2. Circuit diagrams of individual components can be found in Appendix A. The input signal to the frequency tracker first passes through a low pass filter (7.5 MHz cutoff) and a three-stage, wide band video amplifier with variable gain. This instantaneous Doppler signal is then mixed with a local oscillator frequency in a monolithic, balanced modulator operating in a suppressed carrier mode. This results in an upmixing of the instantaneous Doppler

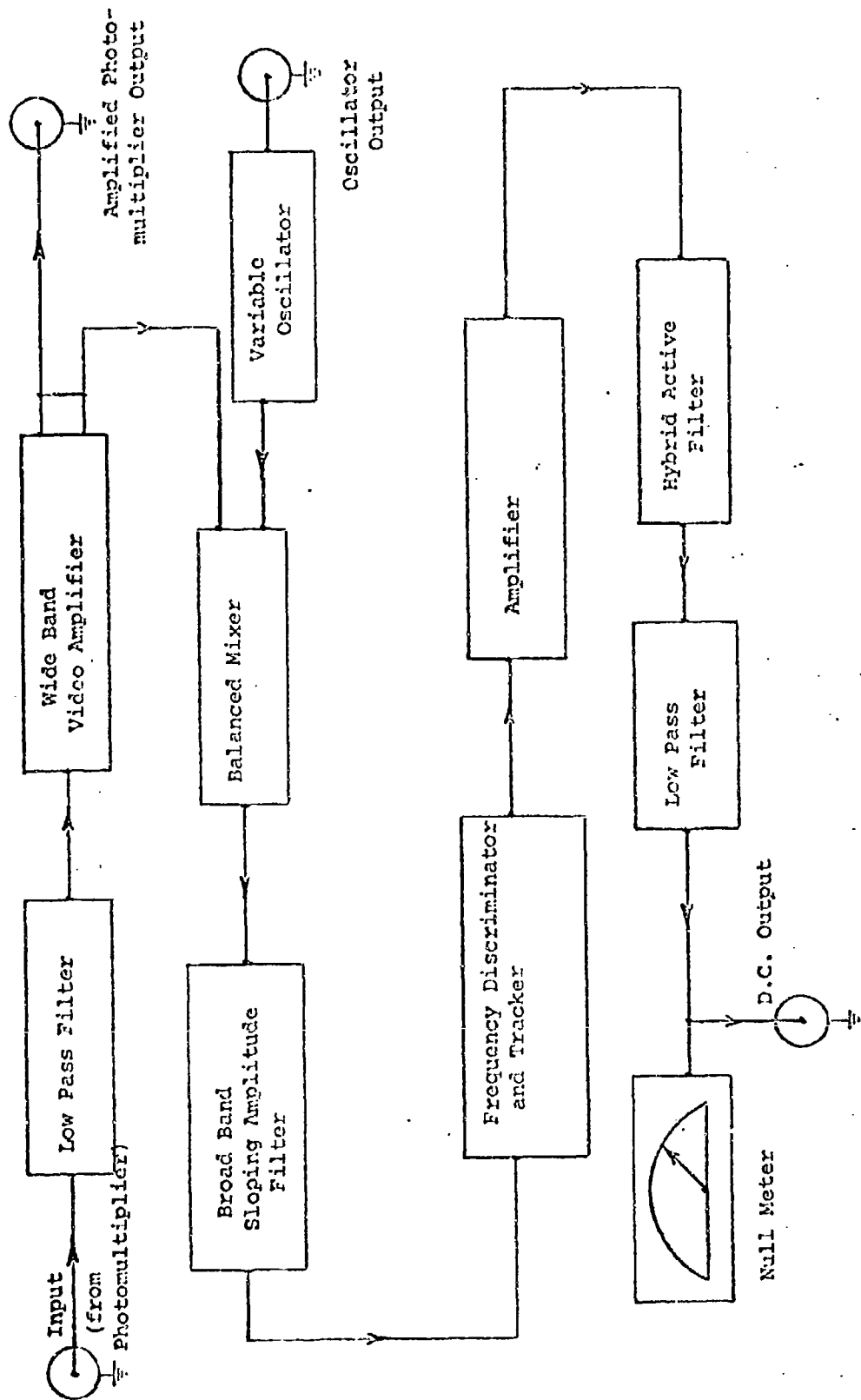


FIGURE 4.2

FREQUENCY TRACKER SCHEMATIC

signal from an average value (at a Reynolds number of 50,000) of around 300 KHZ at the centerline of the pipe to an intermediate frequency (I.F. Frequency) in the range of 9-9.5 MHZ. In the output circuit of the mixer module there is a broad band, sloping amplitude LC filter with a center of about 9.8 MHZ such that the lower side band of the mixed signal is greatly attenuated relative to the upper side band. For example, if a carrier frequency from the local oscillator of 9.1 MHZ is mixed with a 300 KHZ mean Doppler signal, the upper side band of 9.4 MHZ would correspond to the mean frequency (mean velocity) about which there is a frequency modulation. The broad band filter also serves in attenuating most of the noise outside of this I.F. frequency range of interest before the signal is fed into the tracking filter module.

Next, the FM signal enters a sensitive frequency discriminator module which essentially tracks the instantaneous I.F. frequency and provides a D.C. output current proportional to the instantaneous deviation of the I.F. frequency from the fixed center frequency of the phase-locked loop (PLL).

The phase-locked loop integrated circuit, the heart of the tracking filter module, is basically an electronic servo-loop consisting of a phase detector, a low pass filter and a voltage controlled oscillator (VCO). The VCO output is fed back to the phase detector, as well as being the output of the PLL. The VCO is set at a fixed frequency (free running frequency) by an external capacitor. The phase detector compares the phase and frequency of the incoming signal with that of the VCO and generates an output voltage (error voltage) which causes the VCO frequency to change in such a way as to drive the error voltage to zero. That is to say, the PLL is capable of locking or synchronizing with an incoming

signal, with the average voltage applied to the oscillator a function of the incoming signal. With no input signal into the PLL, the error voltage is equal to zero.

Fundamental static and dynamic loop characteristics such as capture range, loop bandwidth, capture time and transient response are controlled primarily by the loop filter and as noted in the Signetics (1973) literature, the filter has the effect of limiting the maximum rate at which tracking can occur. Therefore, if a high tracking rate is needed, the filter should have a high cutoff frequency. There are limitations as to how high this cutoff can be before causing other adverse effects, however. Signetics (1973) suggests typical sweep frequencies in the range of 10^{-3} to 10^{-5} of the I.F. frequency. In the present tracking setup, for an I.F. center frequency of 9.4 MHz, this gives a range of sweep frequencies of 94 to $9.4 \cdot 10^3$ Hz. From optical considerations, the frequency window was shown in the last chapter to be approximately 20 to 1450 Hz, well within the range of the PLL capability.

When the PLL is locked to a signal, the VCO voltage is a function of the frequency of the input signal and is the demodulated output during FM demodulation. The VCO voltage-to-frequency characteristic is linear and in the present design it is this VCO output frequency that is then converted to a voltage through a series of filters. The output of the last filter, and therefore the tracking module, is a D.C. signal with a small AC ripple riding on it at the frequency of the modulated signal. This signal then goes through an amplifier and a low pass filter which filters out the AC signal.

At the final stage of the frequency tracker is another low pass filter. Its cutoff should be sufficiently high to allow the demodulated

signal to pass but it should not be too high that just noise with no more additional information is obtained. In the original design of this tracker the filter had a -3 dB point of approximately 10.9 KHZ which in comparison to the estimated frequency window was much too high. This filter was bypassed and the readout of the frequency tracker went directly to a tape recorder before being processed. The frequency response (2500 HZ) of the Ampex SP-300 tape recorder at a speed of 7 inches per second was found to be sufficiently close to the estimated frequency window.

The output of the last filter is fed into a front panel jack on the tracker from which the demodulated signal can be further processed. This signal is also fed to a front panel D.C. meter, acting as a null meter, which allows the mean Doppler frequency to be readily evaluated. This is accomplished by adjustment of the frequency of the local oscillator until the D.C. level from the frequency tracker and therefore the error voltage from the phase-locked loop are equivalent and, under properly trimmed conditions, equal to zero.

As further explained in Chapter V, the two-component reference beam mode was used for the present experimental effort, in spite of the fact that it was not possible to take full advantage of its signal processing capabilities. In fact, it was not possible to make more than mean frequency (that is, mean velocity) measurements using the frequency trackers. Therefore, the RMS capabilities described in Figure 4.1 were not used. A brief indication of the reason for this is described in the following section.

Frequency Tracker Evaluation

One of the problems that arises in attempting to evaluate the signal processor of an LDV is that of producing a test signal representative of the fluid flow. This encompasses not only providing a simulated Doppler signal that is frequency modulated to represent a turbulent signal but it also requires simulation of normal system noise and the effects of particle size distribution. A test system that comes very close to accomplishing this is indeed possible and is outlined in the following pages.

Wilmsworth (1972) developed a signal generator that gives a sine wave output that is randomly modulated in phase and amplitude by employing pseudo-random noise generators to modulate the sine wave. This signal is then swept by mixing a constant frequency signal with the output of a voltage controlled oscillator, the difference of which is the instantaneous Doppler signal. This signal simulator would be almost complete save for the fact that system noise and particle size, two important factors which effect frequency tracker performance, are not simulated.

In actuality this seemingly complex Doppler signal generator, together with the added capabilities of pseudo system noise, transient signal or noise inputs, and an approximation to particle size distribution, is available with off-the-shelf signal generators and amplitude shaping filters.

One of the key elements in the circuit is a random noise generator comparable to WAVETEK Model 132. This generator contains a pseudo-random sequence generator which produces analog (or digital) noise. The signal is periodic after a variable number of cycles. The bandwidth and the frequency deviation of the noise can be selected as well. This allows this generator to pseudo-randomly frequency modulate a pseudo-mean Doppler

frequency generated by an attendant, in-line, generator, in this case a WAVETEK Model 144. This is made possible by using the VCG input of the Model 144 to externally control the frequency of this second generator. Ideally, a second Model 132 in place of the Model 144 would allow not only a pseudo-random frequency modulation but, in addition, the variable S/N capabilities of the Model 144 would provide a pseudo system noise source riding on the signal.

This so-called simulated Doppler signal needs to be amplitude modulated by passing the noise signal through a shaping filter driven by white noise before it triggers the FM generator. This simulates the variation in light intensity of the Doppler signal during the passing of scattering particles of different sizes through the test volume. Two other important factors should also be considered. Transient signal or noise inputs into the tracker as well as signal dropout, in which there is a momentary lack of signal into the tracker, can be included in the model with the addition of a random pulse generator and a summing amplifier.

A correlator is used in order to obtain the auto-correlation of both the modulation into the tracker and the demodulated output of the frequency tracker. A cross-correlation of the two modulation signals would indicate any variations between them. A Fourier transform of the cross-correlation into the frequency domain by means of a spectrum analyzer, though not essential, would then indicate the range of frequencies where inaccurate demodulation occurs. Such basic analysis of a tracker is considered to be a minimum requirement to assuring the accuracy of all velocity data, other than mean velocity, obtained from a tracker.

In the present evaluation shaping filters were not readily available and only one noise generator was easily obtained. A random pulse

generator was not used either. Despite these limitations informative results could be generated. The circuitry utilized is outlined in Figure 4.3.

As a second noise generator was not available, the effects of variation of the modulation bandwidth and the depth of modulation on the frequency tracker were observed without noise on the signal. Independent of this study the roles of the two generators were reversed in order to assess the behavior of the frequency tracker with variation of the noise level on a constant amplitude, simulated Doppler signal. In this case the modulation was either square or triangular rather than pseudo-random.

None of the correlation results are presented. Instead, the single sweep pictures, which show more graphically the same general trends, are presented. Figures 4.4 and 4.5 give some of the typical results obtained from straight-forward application of the test setup depicted in Figure 4.3 with and without reversing the roles of the two frequency generators. Figure 4.4A shows a typical Doppler signal obtained from the electro-optical receiving elements in a turbulent flow condition. In it one can see not only the mean Doppler frequency and its modulations but also noise.

As the phase-locked loop is, among other things, a band-pass filter, noise outside the PLL bandwidth, though still of concern, is of minor importance in relation to noise on the Doppler signal that is passed by the filter. With this in mind a simple but essential test of the frequency tracker's ability to lock on a modulated signal with noise was attempted. Figures 4.4B and 4.4C demonstrate what occurs when the bandwidth of the modulation (square or triangular, respectively) extends beyond the dynamic lock range of the PLL for a given S/N ratio of the carrier frequency.

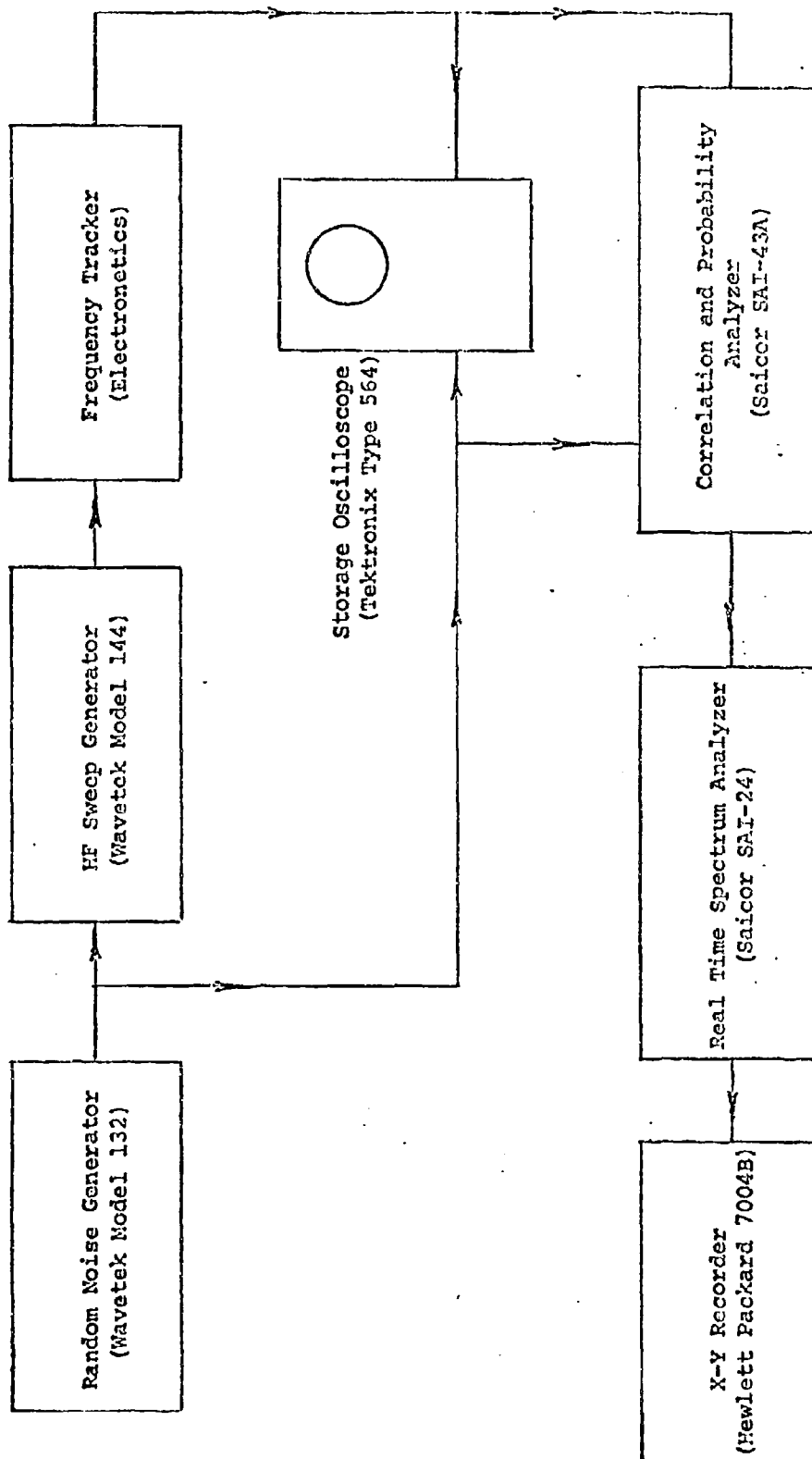


FIGURE 4.3

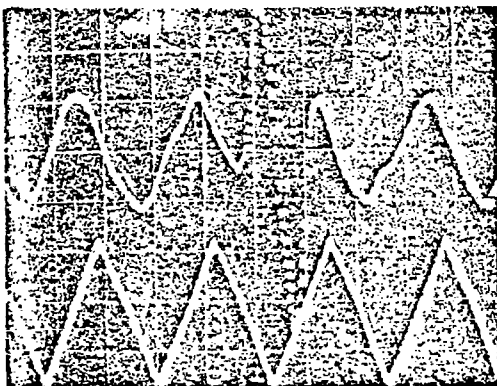
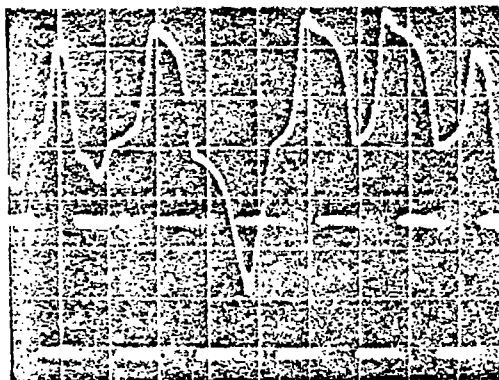
TRACKER EVALUATION CIRCUITRY



A. Real Doppler Signal from Photomultiplier
Mean Frequency: 375 KHZ

B. Square Wave Modulation of Doppler Signal into Frequency Tracker (lower curve). Demodulated Signal Out of Frequency Tracker (upper curve).

Mean Doppler Frequency: 300 KHZ
Sweep Width: ± 30 KHZ
S/N of Doppler Signal: 10 dB
Modulation Frequency: 2 KHZ



C. Triangular Wave Modulation of Doppler Signal into Frequency Tracker (lower curve). Demodulated Signal Out of Frequency Tracker (upper curve).

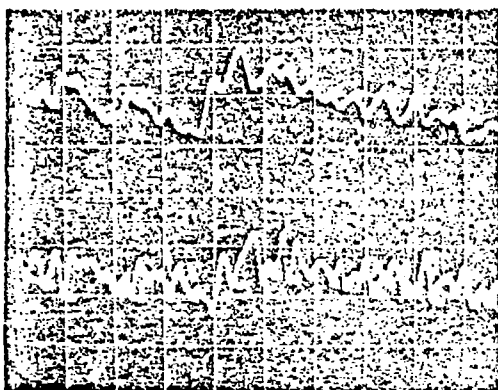
Mean Doppler Frequency: 300 KHZ
Sweep Width: ± 20 KHZ
S/N of Doppler Signal: 4 dB
Modulation Frequency: 2 KHZ

FIGURE 4.4

A REAL DOPPLER SIGNAL AND THE RESPONSE OF THE FREQUENCY TRACKER TO S/N ON A SIMULATED DOPPLER SIGNAL

Reproduced from
best available copy.





- A. Pseudo-Random Frequency Modulation into Frequency Tracker (lower curve).
Demodulated Signal Out of Frequency Tracker (upper curve).

Horizontal Scale: 0.2 ms/div.

Mean Doppler Frequency: 300 KHZ

Sweep Width: ± 50 KHZ

Modulation Frequency: 0-10 KHZ

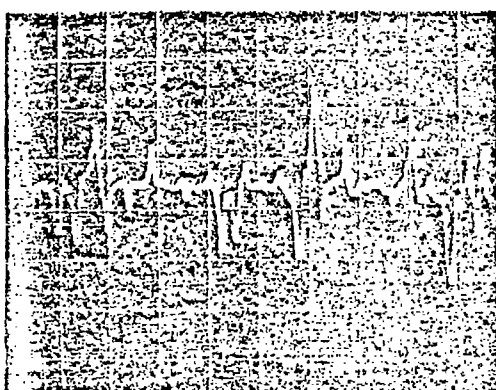
- B. Pseudo-Random Frequency Modulation into Frequency Tracker (lower curve).
Demodulated Signal Out of Frequency Tracker (upper curve).

Horizontal Scale: 1 ms/div.

Mean Doppler Frequency: 300 KHZ

Sweep Width: ± 250 KHZ

Modulation Frequency: 0-10 KHZ



- C. Demonstration of Real Doppler Signal

Horizontal Scale: 0.1 ms/div.

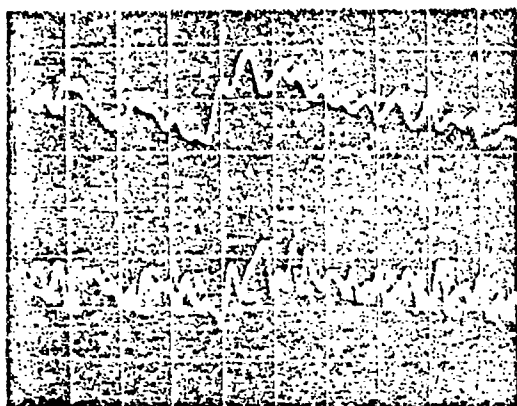
Mean Frequency: 375 KHZ

Reproduced from
best available copy.



FIGURE 4.5

FREQUENCY TRACKER RESPONSE TO SIMULATED, PSEUDO-RANDOM
MODULATION AND REAL DOPPLER MODULATION



- A. Pseudo-Random Frequency Modulation into Frequency Tracker (lower curve).
Demodulated Signal Out of Frequency Tracker (upper curve).

Horizontal Scale: 0.2 ms/div.

Mean Doppler Frequency: 300 KHZ

Sweep Width: ± 50 KHZ

Modulation Frequency: 0-10 KHZ

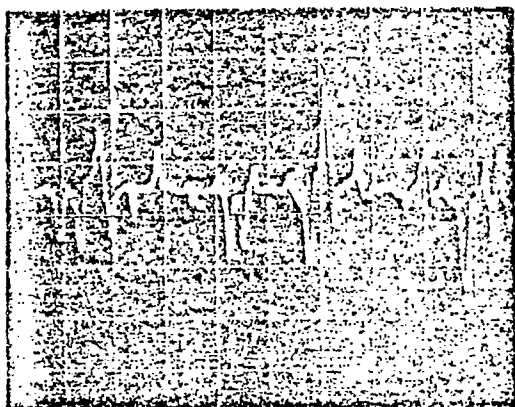
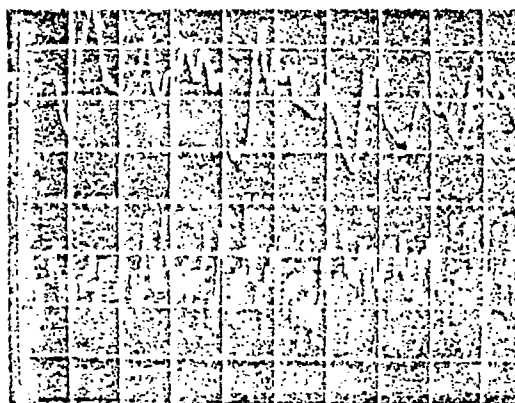
- B. Pseudo-Random Frequency Modulation into Frequency Tracker (lower curve).
Demodulated Signal Out of Frequency Tracker (upper curve).

Horizontal Scale: 1 ms/div.

Mean Doppler Frequency: 300 KHZ

Sweep Width: ± 250 KHZ

Modulation Frequency: 0-10 KHZ



- C. Demonstration of Real Doppler signal

Horizontal Scale: 0.1 ms/div.

Mean Frequency: 375 KHZ

Reproduced from
best available copy.



FIGURE 4.5

FREQUENCY TRACKER RESPONSE TO SIMULATED, PSEUDO-RANDOM
MODULATION AND REAL DOPPLER MODULATION

What is important to observe here is the capability of the tracker to maintain a continuous lock condition down to S/N ratios in the range of 6-10 dB (S/N values between 2 and 3:1) for relatively large frequency fluctuations. It should be noted that the sweep widths in these photographs are only typical cases. Larger excursions were indeed possible for the same range of S/N. Larger modulation frequencies were also possible.

Figures 4.5A and 4.5B show typical frequency response characteristics for, now, a pseudo-randomly modulated Doppler frequency with essentially no noise (S/N = 50 dB). Figure 4.5B shows that a sweep width of 250 KHZ exceeds the dynamic lock range of the PLL. Tests showed that at a mean Doppler frequency of 300 KHZ, with a 0-10 KHZ bandwidth on the random modulation frequency, the lock range of the PLL allowed the equivalent of 50% turbulence intensity fluctuations of the mean frequency. This is more than sufficient for the present application where maximum turbulence intensities of 10-20% were expected. Yet, as Figure 4.5C clearly illustrates, the demodulation of a real Doppler signal is not possible.

The apparent reasons for the poor demodulation characteristics of the present LDV system are varied. The optical considerations discussed in Chapter III are believed to be of particular significance. As determination of the S/N ratio of the real Doppler signal is difficult, if not impossible, to evaluate, no clear indication as to the quality of the optical signal is available. The noise characteristics of the photomultiplier tube are known to be of influence. The modifications suggested in Chapter III could not but enhance the signal quality as well as improve the other characteristics outlined.

Signal dropout and transient signal or noise inputs are other factors to consider. Preliminary applications of a pulse generator to simulate transient signals indicated good performance of the tracker though the observed stability of the phase-locked loop shows the need for a slightly more overdamped loop response. In addition, the AC output of the tracker should go to zero during the non-burst intervals. This was not possible to observe as there is no signal dropout protection electronics in the present tracker. In modifying the electronics, the effect of the signal dropout addition would have to be analyzed for its effect on accurate frequency demodulation. Further analysis is needed of this LDV system and possible alternatives, before accurate and complete demodulation of higher moments of the Doppler signals can be assumed possible.

CHAPTER V

MEASUREMENTS AND OBSERVATIONS IN A POLYMER FLOW

The stated goals of this part of the work were, as already noted, two-fold. Polymer drag degradation data in low polymer concentration pipe flows with an in-line centrifugal pump was desired. Secondly, with the fresh polymer (before passing through the pump), mean velocity profile measurements of the same polymer concentrations were made.

Since no work has been published using a centrifugal pump and since it was anticipated that it would cause dramatic degradation of the polymer, it was desired to document this degradation as a function of the number of passes of the flow through the pump. Low concentrations of polymer are of particular interest for their potential applications and yet few degradation results in a flow system have been reported. Most authors have generally worked with large and, many times, saturated concentrations (see, for example, the data summary in Virk et al., 1970). Goren and Norbury (1967) worked with low concentrations but did only single pass measurements of drag reduction. Huang (1974) also worked with extremely low concentrations. His interest was in developing similarity laws for undegraded, unsaturated polymer flows. Sylvester and Kumor (1973) performed some degradation tests but their lowest concentration was 50 ppm.

Various velocity profile models demonstrate that differences are expected between the velocity distributions for drag reducing and Newtonian fluids, with particular interest centered on the near-wall-

region. Goren and Norbury (1967) ran low concentration velocity profiles in a 5.08 cm diameter pipe using a pitot tube.

Drag Reduction Degradation Studies

Drag reduction was measured as a pressure loss by means of two side-wall pressure taps located 362 cm apart, the pressure difference being measured by an ITT Barton differential pressure transducer. In measuring the pressure loss in a polymer run it was found that due to the small settling tank upstream of the pressure taps, it took approximately two minutes after injection for the polymer to record a minimum pressure drop (maximum drag reduction) at a Reynolds number of 50,000. This was considered, therefore, the minimum allowable time before taking pressure or velocity profile readings.

The percentage drag reduction was calculated by the relationship

$$\% \text{ Drag reduction} = \left(1 - \frac{F_p}{F_s}\right) \cdot 100 \quad (5.1)$$

where F_p is the friction factor of the polymer plus solvent as measured by a pressure reading during a particular polymer run and F_s is the friction factor with the solvent alone, in this case water, both being measured at the same Reynolds number, $R_N = \frac{VD}{\nu}$. With the wall shear stress, τ_w , given by

$$\tau_w = \frac{D}{4} \frac{dp}{dx} \quad (5.2)$$

where D is the diameter of the pipe and $\frac{dp}{dx}$ is the pressure gradient measured across the pressure transducer, F can be found from the formula

$$F = \frac{2D}{\rho V^2} \frac{dp}{dx} \quad (5.3)$$

with ρ as the fluid density and V as the mean velocity of the flow. For

the low concentrations tested, ρ was assumed to be that of water. The temperature was closely monitored, however, as the kinematic viscosity, ν , is quite sensitive to temperature. A one degree centigrade error in temperature results in approximately 0.75% error in mean velocity for the range of temperatures (14-20° C) encountered.

Maximum drag reduction studies were made for 10, 20, and 40 ppm (by weight) concentrations of Separan AP-30 polymer. Maximum drag reductions and their corresponding friction velocities, $V_T = \left(\frac{\tau_w}{\rho} \right)^{\frac{1}{2}}$ and friction factors, F , at three Reynolds numbers ($4 \cdot 10^4$, $5 \cdot 10^4$, $6 \cdot 10^4$), are presented in Table 5.1. The ratio of maximum to average velocity for a R_N of 50,000 is also shown for the three polymer concentrations as well as for fresh water. The maximum drag reductions for these concentrations are plotted in Figure 5.1. The highly non-linear nature of the relationship between polymer concentration and the maximum drag reduction is quite evident, where it is seen that drag reduction is directly proportional to the polymer concentration raised to the one-half power.

As can be seen from the three curves there is also a non-linear relationship between the Reynolds number and the percentage drag reduction. For increasing Reynolds number the pressure drop is not increasing as rapidly as for the case of the pure solvent. This is seen in Table 5.1 in the values of F for any of the polymer flows and the fresh water flow at the same Reynolds number. For Reynolds numbers greater than 60,000 it is expected that the maximum drag reductions would be even more dramatic.

A representative measure of the repeatability and percentage error of the pressure readings and the mean flow velocities can be obtained

TABLE 5.1

DRAG REDUCTION PARAMETERS

Polymer Concentration (ppm)	Average R_N	Maximum Drag Reduction (%)	$\frac{V_{max}}{V_{average}}$	V_t (cm/sec)	F
0	40,000	0	---	4.66	.0218
	50,000	0	1.17	5.67	.0209
	60,000	0	---	6.58	.0193
10	40,000	23	---	3.84	.0167
	50,000	25	1.27	4.67	.0157
	60,000	29	---	5.23	.0137
20	40,000	35	---	3.55	.0142
	50,000	36	1.19	4.32	.0134
	60,000	40	---	4.73	.0112
40	40,000	45	---	3.48	.0119
	50,000	49	1.13	4.12	.0106
	60,000	54	---	4.49	.0088

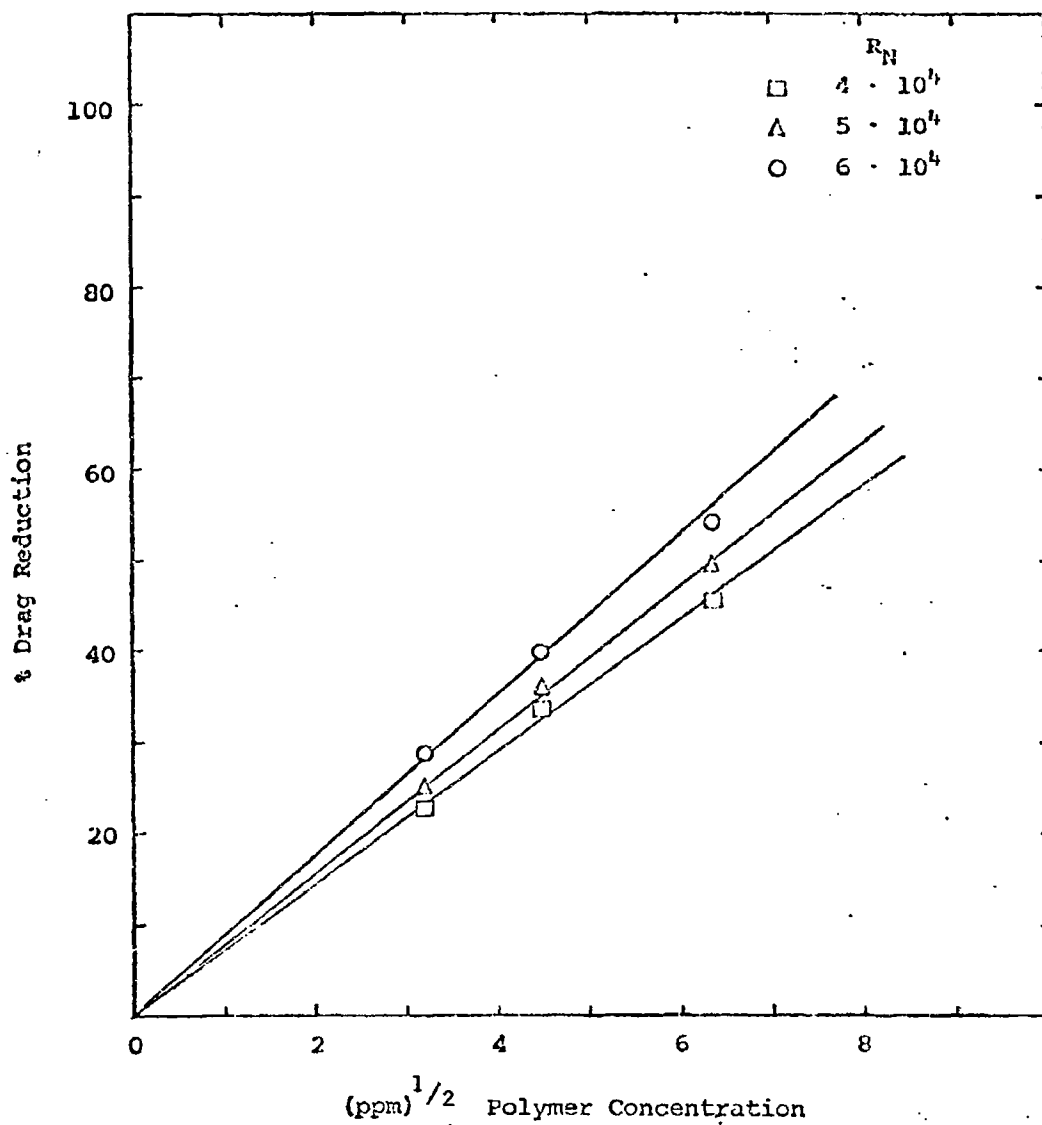


Figure 5.1 Maximum Drag Reductions for Low Polymer Concentrations

from the values of the friction factor for water acquired on six separate occasions during the testing period. The experimentally obtained values are given in Table 5.2. The average deviation from the average of 0.0209 is 1.5%. This included a 1.3% average deviation in the pressure readings (based on the Moody diagram) and a 1% average deviation in velocities. From the Blasius equation the friction factor is calculated to be 0.0210 for $R_N = 50,000$.

TABLE 5.2

VALUES OF THE FRICTION FACTOR (F)
FOR FRESH WATER AT $R_N = 5 \cdot 10^4$

Run	F_{water}	% Deviation from average *
1	.0210	0.5
2	.0203	2.7
3	.0214	2.5
4	.0209	0.0
5	.0205	1.8
6	.0212	1.5

* $F_{\text{average}} = 0.0209$

One method for assessing polymer degradation, while continually evaluating the drag reduction effectiveness of the polymer solutions, is to measure the friction factor as a function of the flow time. With the polymer solution being continually sheared in a turbulent flow, sufficient degradation eventually occurs resulting in increased pressure

gradient requirements to maintain a given flow rate. This is clearly demonstrated in Tables 5.3, 5.4, and 5.5 where polymer degradation in terms of the decrease in the percent of drag reduction of a particular polymer concentration is tabulated. The solution was repeatedly passed through the flow system until it no longer was effective as a drag reducing agent.

Polymer concentrations of 10, 20, 40, 50, and 100 ppm were used. However, due to the limitations of the flow system as described in Chapter II, it was not possible to dissolve concentrations greater than 40 ppm before the solution arrived at the test area. Therefore, maximum drag reduction readings for the 50 and 100 ppm concentrations could not be obtained. It was assumed that these solutions were well dissolved further downstream before passing through the centrifugal pump for the first time.

A few general observations can be made. The hydrodynamic interaction between the polymer and the flow field is significant not only in terms of the drag reduction effectiveness but also in relation to the severity of the polymer degradation. For a saturated or over-saturated solution the drag reduction is not only a maximum but it is not reduced in effectiveness until the concentration of high molecular weight molecules is decreased, by degradation, below that required for maximum drag reduction. As the concentrations used in the present experiments were all undersaturated (see Huang, 1974), maximum drag reduction, estimated by Virk et al., (1970) was not obtained and degradation began almost immediately in the high shear environment. The shear stresses caused by the centrifugal pump cause the breaking of chemical bonds and the degradation of polymer solutions passing through it. Unfortunately the pump

TABLE 5.3
PERCENT DRAG REDUCTION AS A FUNCTION OF PASSES
THROUGH THE SYSTEM FOR $R_N = 4 \cdot 10^4$

ppm Polymer	Number of Passes Through System						
	0	1	2	3	4	5	6
10	23	7	0	---	---	---	---
20	35	3	0	---	---	---	---
40	45	11	5	0	---	---	---
50	*	17	7	0	---	---	---
100	*	28	23	19	12	6	0

* Maximum drag reductions not available.

TABLE 5.4

PERCENT DRAG REDUCTION AS A FUNCTION OF PASSES
THROUGH THE SYSTEM FOR $R_N = 5 \cdot 10^4$

ppm Polymer	Number of Passes Through System						
	0	1	2	3	4	5	6
10	25	0	---	---	---	---	---
20	36	0	---	---	---	---	---
40	49	12	5	0	---	---	---
50	*	12	6	0	---	---	---
100	*	32	26	20	11	7	0

* Maximum drag reductions not available.

TABLE 5.4

PERCENT DRAG REDUCTION AS A FUNCTION OF PASSES
THROUGH THE SYSTEM FOR $R_N = 5 \cdot 10^4$

ppm Polymer	Number of Passes Through System					
	0	1	2	3	4	5
10	25	0	---	---	---	---
20	36	0	---	---	---	---
40	49	12	5	0	---	---
50	*	12	6	0	---	---
100	*	32	26	20	11	7

* Maximum drag reductions not available.

TABLE 5.5

PERCENT DRAG REDUCTION AS A FUNCTION OF PASSES
THROUGH THE SYSTEM FOR $R_N = 6 \cdot 10^4$

ppm Polymer	Number of Passes Through System						
	0	1	2	3	4	5	6
10	29	0	---	---	---	---	---
20	40	0	---	---	---	---	---
40	54	12	4	0	---	---	---
50	*	10	4	0	---	---	---
100	*	33	27	20	11	7	0

* Maximum drag reductions not available.

performance with a particular polymer concentration could not be categorized because the drag reduction properties of the circulating polymer solution were changing with every pass through the pump. From the 50 and 100 ppm runs the asymptotic, non-linear degradation of the polymer is quite evident.

Tables 5.3, 5.4, and 5.5 show that drag reduction is a function of R_N . The higher the flow rate the more effective is the drag reduction and, in turn, the higher is the degradation rate. This is quite apparent from the first and second pass drag reductions for all concentrations. Looking at Table 5.3, even the 10 ppm solution has some drag reduction capabilities after one pass through the pump for the lowest R_N tested. However, for the existing test conditions, the low polymer concentrations of 10, 20, 40 and 50 ppm suffered considerably greater losses in drag reduction effectiveness with the first pass through the pump than did the 100 ppm solution. They suffered a 50-60% degradation in drag reduction while the 100 ppm solution degraded only 18% for all Reynolds numbers. For subsequent runs the 100 ppm solution degraded at an ever increasing rate with, again, more severity at the higher R_N .

As was already noted in Chapter I, the concentration of the highest molecular weight elements in the molecular weight distribution influences the degradation characteristics of a particular polymer flow. With increasing concentration of a given polymer, the probability of entanglement between polymer chains increases. What apparently occurs is that with the first pass through the pump, the concentration of the higher molecular weight elements in the 10 and 20 ppm solutions experiences complete scission. For the 40 and 50 ppm solutions there is almost complete scission. In the 100 ppm solution this complete scission does not occur

as rapidly and, in fact, is postponed until approximately the fourth or fifth pass through the pump. The drag reduction capabilities that remain after this are, as for the cases of the lower concentrations, possibly due to factors other than entanglement of the high molecular weight chains. As noted by Sylvester and Kumor (1973), this residual resistance to shear is present in infinite dilution solutions and at this point just the interaction between solvent and polymer chains is capable of bringing about complete shear degradation. As they also note, extreme caution must be taken in interpreting experimental results because of both the chemical and mechanical factors that effect the shear degradation. Some of these were noted in Chapter I.

In all of the above pressure results it was assumed that there were no pressure errors due to the viscoelastic properties of the polymer. Broadbent et al. (1968) suggested that a systematic error, independent of hole size, exists for viscoelastic fluids for Reynolds numbers well below 50. Here the Reynolds number based on the undisturbed wall shear stress, τ_w , and the hole diameter, d , (in this case approximately 3.1 mm) can be written as $R_N = \frac{d}{\nu} \left(\frac{\tau_w}{\rho} \right)^{\frac{1}{2}}$ (see Tanner and Pipkin, 1969). For the present experiments R_N was calculated to be approximately 230.

Velocity Profile Results

Axial mean velocity profiles for water and 10, 20 and 40 ppm solutions of Separan AP-30 at a Reynolds number of 50,000 were obtained. The two-component reference beam mode described in Chapter III was used to obtain the velocity results. The output of either of the photomultiplier channels could be used for this. As a check on results, however, both channels were used sequentially at each data station. This proved very useful in checking for consistency of results. This was necessary

as occasionally the frequency tracker would come out of a lock mode (i.e. not locked on a Doppler signal) and would give an erroneous reading. With good operation, there was a constant difference in Doppler signals read between the two channels (2% difference for the centerline value) attributable to a slight misalignment in the optic systems. As misalignment was assessed to be axi-symmetric, the average of the two signals was used to give the mean Doppler and therefore mean velocity readings. It should be noted that all frequency detectors yield the absolute magnitude of the frequency, losing the sign. Therefore, care should be used in calculating the velocity using equation (3.1).

The results are plotted in Figure 5.2 where the velocities have been normalized by the maximum (centerline) velocities measured during each test run. They are plotted versus a normalized distance from the wall, $\bar{r} = 1 - \frac{r}{a}$, where r is the distance from the flow centerline axis and a is the radius of the pipe. The fresh water profile compares well with the mean velocity profile of Sandborn (1955) who measured air flow in a 10.16 cm diameter pipe at a Reynolds number of 50,000.

The velocity profiles become fuller with the velocity defect reduced at a similar radial position in the pipe for increasing polymer concentrations. There appears to be a crossover point between the polymer profiles and that of water at an \bar{r} between 0.03 and 0.04. This is quite close to the 0.05 value obtained by Walter (1974) and Aquino and Lamontagne (1973). Walter worked with a family of variable molecular weight polymers at a concentration of 5000 ppm while Aquino and Lamontagne measured the velocity profiles of water and a 2 ppm solution of POLYOX WSR-301. Similar to the present results, both observed fuller profiles with a decrease in shear rate, dV/dy , close to the wall for the polymer

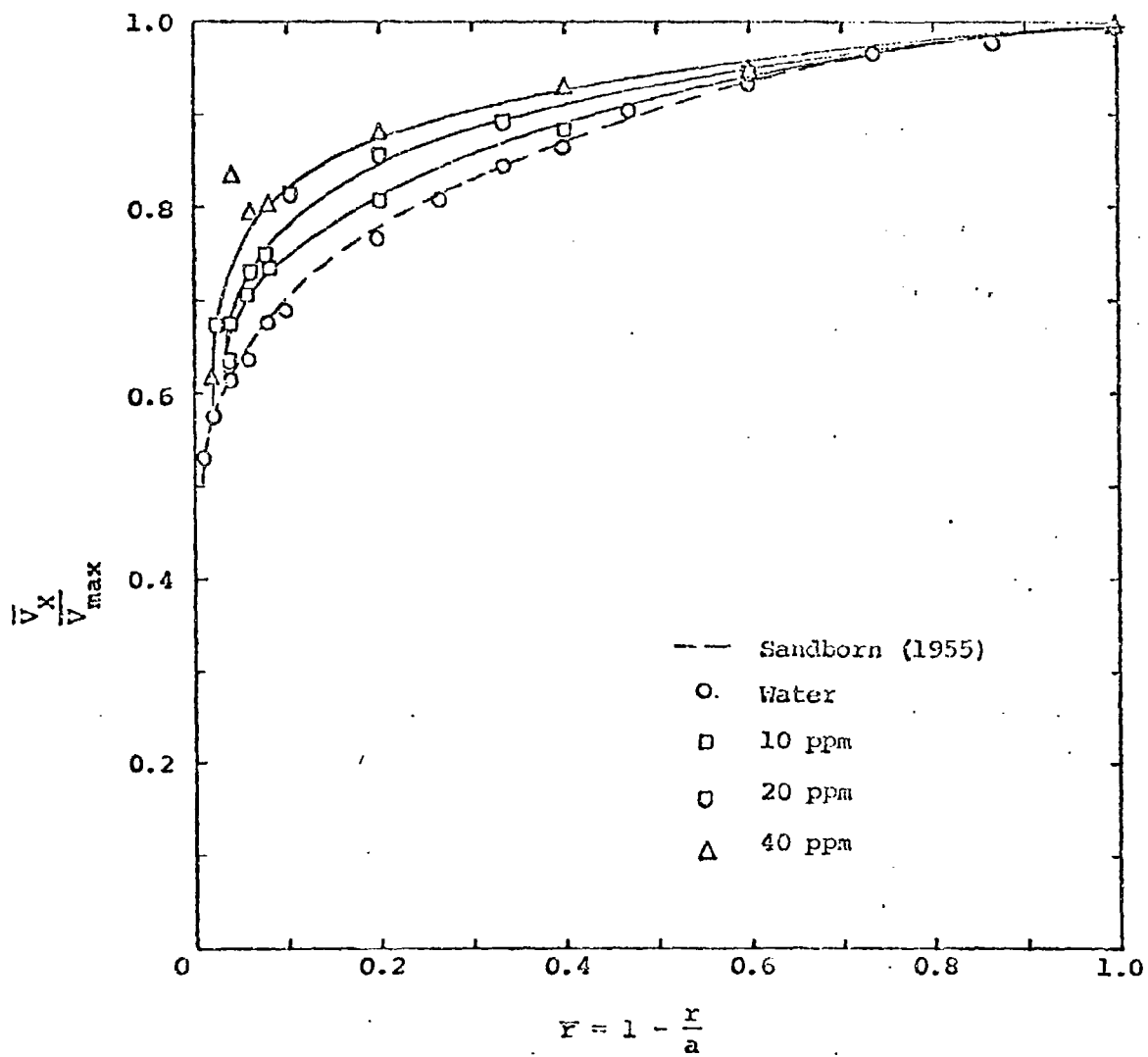


FIGURE 5.2

AXIAL MEAN VELOCITY PROFILES AT $R_N = 5 \cdot 10^4$

solutions. This disparity with Newtonian behavior is still not completely understood. Bryson et al. (1971) who arrived at similar results suggest a quantitative model for the apparent thickening or reduction in the mean velocity of the flow zone near the wall of their 25.4 mm diameter pipe. From measurements within less than 0.1 mm from the wall they observed what appears to be a wall-absorption-type effect of the polymer. In their model it is assumed that this leads to the formation of an essentially stationary and very thin layer at the wall outside of which the regular boundary layer develops. They show that the values obtained for this layer thickness are in agreement with the increase in sublayer thickness necessary to explain their observed decrease in shear rates with drag reduction. Aquino and Lamontagne (1973) show what appears to be a similar stationary layer close to the wall in their polymer profile results.

Though, as will be noted below, it was not possible in the present experiments to obtain results close enough to the wall to observe this possible layer, the above results and the model of Bryson et al. would explain the reduction of the wall shear velocity with the fuller polymer profiles.

The velocity profile data was also normalized by the average velocity of the flow acquired from flow meter readings and then plotted versus \bar{r} . There was again a crossover point of the polymer profiles with that of water at the same \bar{r} . An integration of these velocity profiles showed that the average deviation from the average area under these profiles was 2.5%. The largest deviation was +5% for the 10 ppm profile. For simplification in carrying out this integration it was assumed that near the wall the polymer profiles formed a line of infinite shear rate

beginning at their crossover point with the water profile.

Figure 5.3 shows the same data plotted in a more useful form using dimensionless Newtonian velocity profile laws. The experimentally determined wall shear velocities presented in Table 5.1 were used in preparing these profiles. The well known Newtonian velocity profiles given by equations (5.4) and (5.5)

$$v^+ = y^+ \quad \text{viscous sublayer} \quad (5.4)$$

$$v^+ = 5.62 \log y^+ + 5.0 \quad \text{law of the wall} \quad (5.5)$$

were also plotted. The velocity profiles showed the behavior predicted by the displacement models for low drag reducing flows in which the amount of displacement from the Newtonian line varied proportionately to the polymer concentration. Physically this can be seen from the effective slip model proposed by Virk et al., (1970). In this model the mean velocity profile, V_p , in a polymer solution is given to be the sum of the Newtonian profile velocity, V_N , (at the same friction velocity, V_T , as the polymer solution) plus a constant effective slip velocity, S , both taken at the same Reynolds number. Nondimensionally,

$$V_p^+ = V_N^+ + S^+ \quad (5.6)$$

The zone in which this effective slip occurs is called the interactive zone which in the limit of maximum drag reduction extends to the centerline of the pipe. Virk's maximum drag reduction curve,

$$v^+ = 30 \log y^+ - 20.2 \quad (5.7)$$

is also shown.

In the present low drag reduction results there are few data points which hook up with the viscous sublayer plot. The closest to the wall possible was a $y^+ = 10$ value (0.25 mm from the wall) for the pure solvent.

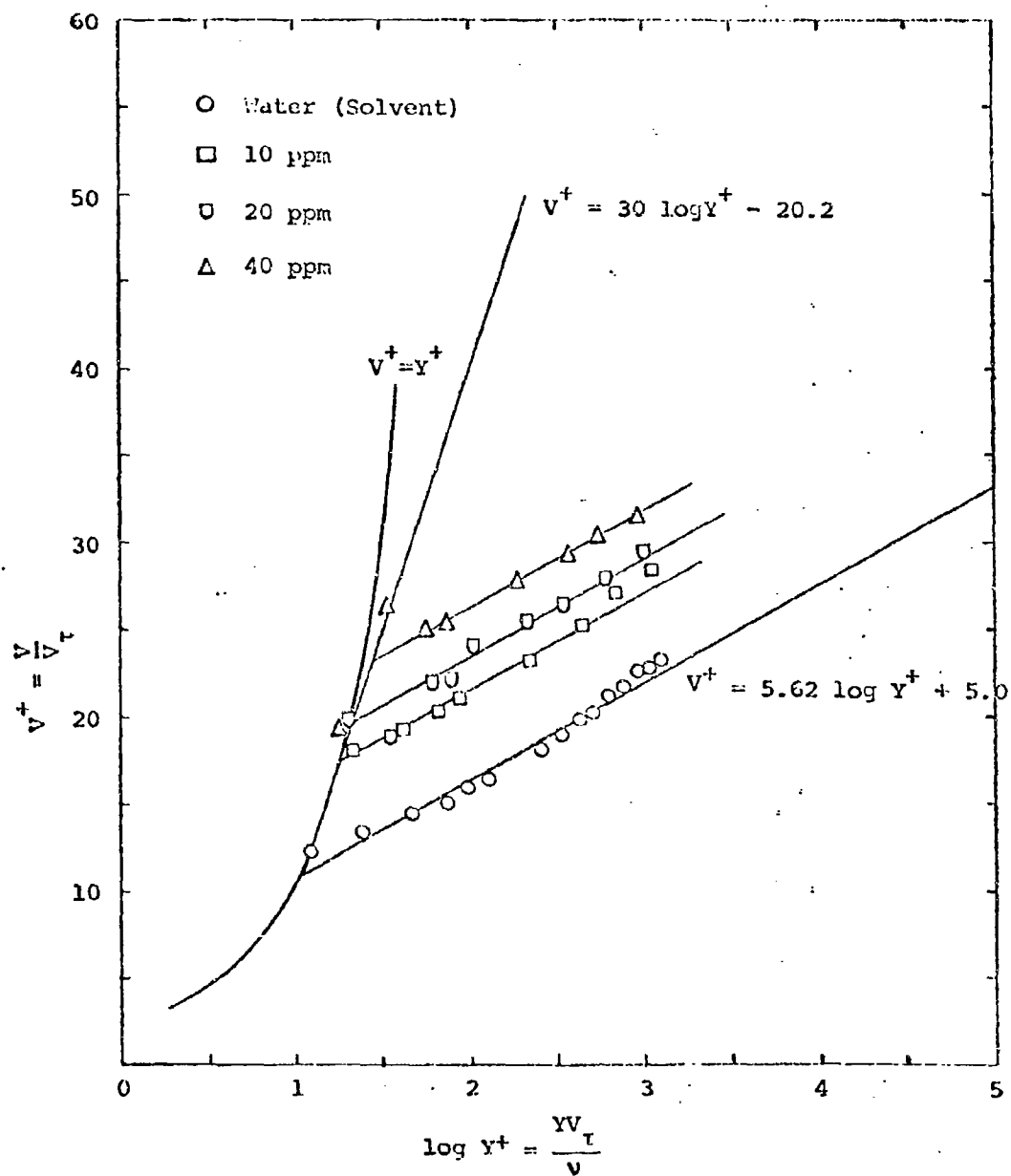


Figure 5.3 Experimental Dimensionless Polymer Velocity Profiles

A 5.03 cm diameter pipe at the Reynolds numbers of interest did not offer a very thick sublayer to span. For the polymer solutions it was not possible to get any closer than $Y^+=18$, approximately the outer limits of the viscous sublayer for the 10 and 20 ppm solutions as seen in Figure 5.3. The frequency tracker was not able to follow signals at distances closer to the pipe wall.

A combination of optical and electronic limitations are considered to have caused this behavior. A design characteristic of the frequency tracker used is that it cannot track mean Doppler frequencies below approximately 170 KHZ. The mean Doppler frequency for the $Y^+=10$ data point was approximately 200 KHZ. Looking at the trends of the polymer velocity profiles in Figure 5.2, to get as close to the wall as for the solvent would imply a mean velocity approaching the minimum that can be tracked by the frequency tracker. The presence of the polymer in solution as well as the proximity of the wall might also have resulted in a Doppler S/N level below the threshold level of the frequency tracker. It is also suspected that the 40 ppm data point that falls on the maximum drag reduction line, but above the other 40 ppm points, is due to erroneous readings caused by the proximity of the wall.

CHAPTER VI

CONCLUSIONS

Drag reduction, effects of polymer degradation and mean flow characteristics of a series of drag reducing polymer flows using tap water as the solvent were obtained using a laser Doppler velocimeter and a pressure transducer.

A closed-loop flow system, using a centrifugal pump for recirculation of the flow, allowed a study of the degradation of the 10, 20, 40, 50 and 100 ppm concentrations of Separan AP-30 polymer injected into the flow. Results indicate a significant degradation for all concentrations after just one pass through the flow system. For subsequent passes through the system the non-linear degradation of the polymer flow is observed asymptotically approaching the wall shear stress value of water.

Velocity profiles at maximum drag reduction for 10, 20 and 40 ppm concentrations were obtained. Data was acquired to within $Y^+ = 10$ of the wall with the LDV system used. Agreement with trends predicted by velocity profile displacement models for low drag reduction flows is demonstrated. With increasing concentration the velocity profiles become progressively fuller. An accompanying decrease in wall shear stress with increased polymer concentration is attributed to a possible stationary layer close to the wall observed by several authors.

An analysis of the optical system used was also presented. It was found, based on fundamental optical considerations as well as from data

on scattering particle densities, that scattering from the natural contaminants in the water was sufficient to ensure that additional scattering particles were not necessary. Signal broadening and signal-to-noise considerations indicated that the dual-scatter mode might improve the signal quality of the LDV system.

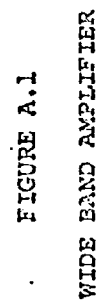
A complete description of the signal processing system was given. The frequency tracker was evaluated in order to obtain some guidelines as to its capabilities and limitations. Results show good performance characteristics within the ranges of expected signal parameters. The tracker is shown, however, to be not capable of accurately measuring more than the mean Doppler frequency signals. To improve this performance specific modifications in the optical system as well as the frequency tracker are suggested. The components of a proposed test circuit to simulate real Doppler signals and to test the accurate and complete demodulation capabilities of any frequency tracker was outlined.

APPENDIX

FREQUENCY TRACKER CIRCUITRY

A general description and a block diagram of the Electronics frequency tracker used was presented in Chapter IV. Detailed circuit diagrams of four of the components which comprise this tracker are shown in Figures A.1, A.2, A.3 and A.4.

Referring to Figure 4.2, the Variable Oscillator is a KHRON-HITE Test Oscillator Model 4200 providing sine wave signals from 10 HZ to 10 MHZ. The Variable Gain Amplifier is a PHILBRICK Differential Operational Amplifier Model P65A. This plug-in module was modified by addition of a trimpot in order to allow adjustment of the gain. The input Low Pass Filter is an epoxy-embedded module with a 10 MHZ cutoff. It was designed to attenuate noise above this frequency. The output, epoxy-embedded Low Pass Filter, as discussed in Chapter IV, has a -3 dB point of approximately 10.9 KHZ. The Broad Band Sloping Amplitude Filter was described in Chapter IV.



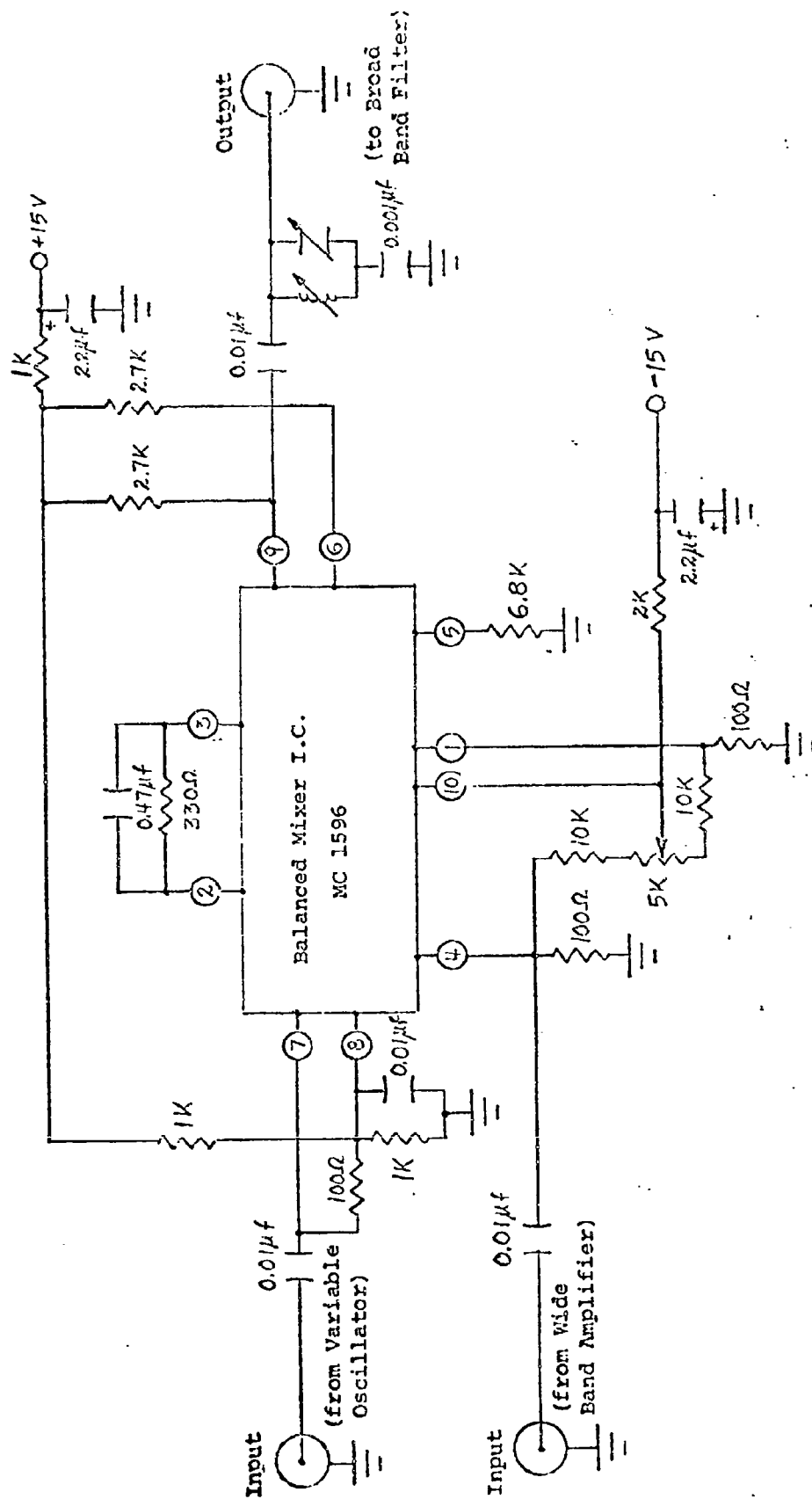


FIGURE A.2

BALANCED MIXER

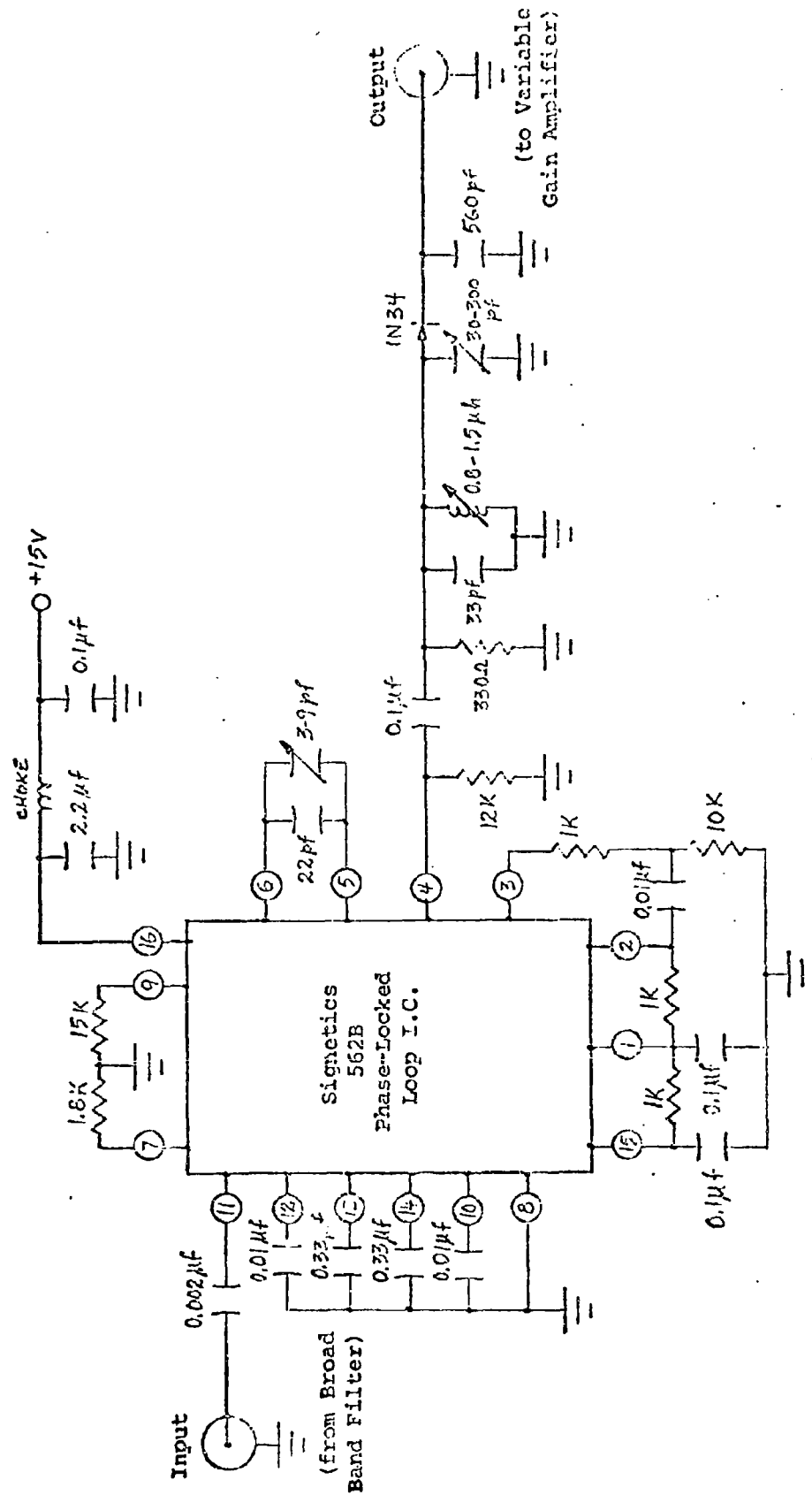


FIGURE A.3

FREQUENCY DISCRIMINATOR AND TRACKER

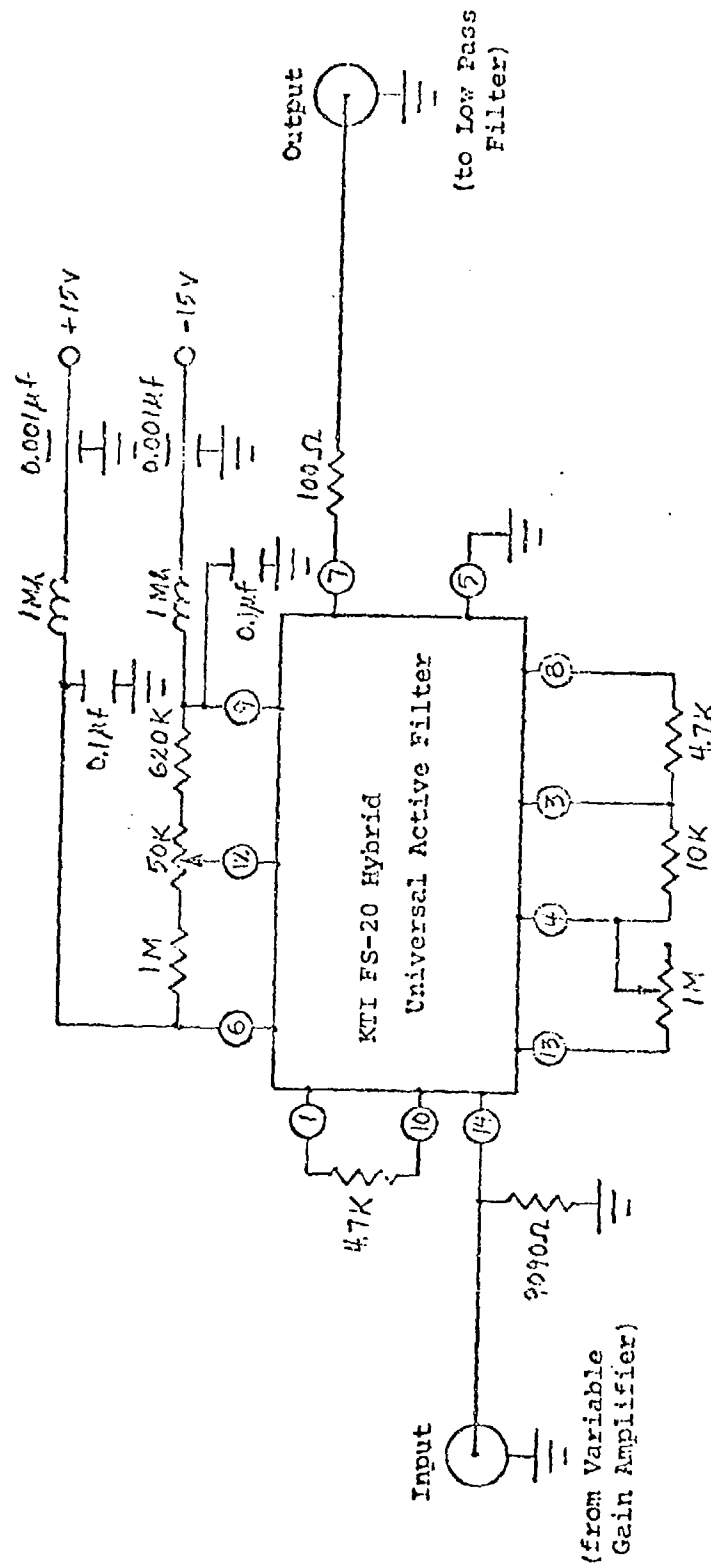


FIGURE A.4

HYBRID ACTIVE FILTER

REFERENCES

- Aguino, H., and Lamontagne, R. "A Method for Measuring the Sublayer Velocity-Profile of a Liquid with Polymer Additive," AIAA Paper No. 73-39, AIAA 9th Annual Meeting and Technical Display, Washington, D.C., January 1973.
- Barker, Steven J. "Laser-Doppler Measurements on a Round Turbulent Jet in Dilute Polymer Solutions," Journal of Fluid Mechanics 60:4 (October 1973): 721-731.
- Berman, N.S.; Gurney, G.B.; and George, W.K. "Pitot Tube Errors in Dilute Polymer Solutions," The Physics of Fluids 16:9 (September 1973): 1526-1528.
- Brayton, D.B., and Goethert, W.H. "A New Dual-Scatter Laser-Doppler Velocity Measuring Technique," ISA Transactions 10:1 (1971): 40-50.
- Brayton, D.B.; Kalb, H.T.; and Crossway, F.L. A Two-Component, Dual-Scatter Laser Doppler Velocimeter With Frequency Burst Signal Readout, in The Use of the Laser Doppler Velocimeter for Flow Measurements (Proceedings of a workshop at Purdue University, March 1972).
- Broadbent, J.M.; Kaye, A.; Lodge, A.S.; and Vale, D.G. "Possible Systematic Error in the Measurement of Normal Stress Differences in Polymer Solutions in Steady Shear Flow," Nature 217:5123 (1968): 55-56.
- Bryson, A.W.; Arunachalam, V.R.; and Fulford, G.D. "A Tracer Dispersion Study of the Drag-Reduction Effect in a Turbulent Pipe Flow," Journal of Fluid Mechanics 47:2 (1971): 209-230.
- Chung, Jin Soo, and Graebel, W.P. Laser Anemometer Measurements of Turbulence in Non-Newtonian Pipe Flows. University of Michigan, College of Engineering, Department of Mechanical Engineering, ORA Project Report 065050) Ann Arbor, Michigan, November 1969.
- Donohue, G.L.; Tiederman, W.G.; and Reischman, M.M. "Flow Visualization of the Near-Wall Region in a Drag-Reducing Channel Flow," Journal of Fluid Mechanics 56:3 (1972): 559-575.
- Brain, L.E. "Coherent and Noncoherent Methods in Doppler Optical Beat Velocity Measurement," Journal of Physics D: Applied Physics 5 (1972): 481-495.

- Dunning, J.W., and Berman, H.S. "Pipe Flow Measurements of Turbulence and Ambiguity Using Laser-Doppler Velocimetry," Journal of Fluid Mechanics 61:2 (1973): 289-299.
- Durst, F.; Melling, A.; and Whitelaw, J.H. "Laser Anemometry: A Report on EUROMECH 36," Journal of Fluid Mechanics 56:1 (1972): 143-160.
- Durst, F., and Whitelaw, J.H. "Light Source and Geometrical Requirements for the Optimization of Optical Anemometry Signals," Opto-electronics 5 (1973): 137-151.
- Eckelman, Larry D.; Fortuna, Giload; and Hanratty, T.J. "Drag Reduction and the Wavelength of Flow-oriented Wall Eddies," Nature Physical Science 236:67 (April 10, 1972): 94-96.
- Edwards, Robert V., and Angus, John C. "Spectral Analysis of the Signal from the Laser Doppler Flowmeter: Time-Independent Systems," Journal of Applied Physics 42:2 (February 1971): 837-850.
- Ellis, A.T., and Ting, R.Y. "Some Storage and Shear History Effects on Polymeric Friction Reduction," Journal of Hydronautics 6:2 (July 1972): 66-76.
- Freihe, C.A., and Schwarz, W.H. "The Use of Pitot Static Tubes and Hot-Film Anemometers in Dilute Polymer Solutions," in Proceedings of the Symposium on Viscous Drag Reduction edited by C.S. Wells. New York: Plenum Press (1969): 281.
- Gadd, G. "Differences in Normal Stress in Aqueous Solutions of Turbulent Drag Reducing Additives," Nature 212 (1966): 1348-1352.
- George, W.K. Analysis of Turbulent Flow Measurements from LDV Data, in The Use of the Laser Doppler Velocimeter for Flow Measurements (Proceedings of a workshop at Purdue University, March 1972).
- George, William K. Jr. "The Measurement of Turbulence Intensities Using Real-Time Laser Doppler Velocimetry." Paper presented at the 2nd International Workshop on Laser Velocimetry, Purdue University, March 1974.
- George, W.K., and Lumley, J.L. Doppler Ambiguity and the Measurement of Turbulence, in The Use of the Laser Doppler Velocimeter for Flow Measurements. (Proceedings of a workshop at Purdue University, March 1977).
- George, William K., and Lumley, John L. "The Laser-Doppler Velocimeter and its Application to the Measurement of Turbulence," Journal of Fluid Mechanics 60:2 (1973): 321-362.
- Coren, V., and Norbury, J.F. "Turbulent Flow of Dilute Aqueous Polymer Solutions," (Transactions of the ASME, December 1967) Journal of Basic Engineering (1967): 814-822.

- Cuenterberg, Gordon Lee Laser-Doppler Anemometer Measurements of Turbulence in Drag Reducing Flows. (University of Michigan, College of Engineering, Department of Engineering Mechanics, ORA Project 065050) Ann Arbor, Michigan, December 1972.
- Huang, T.T. "Similarity Laws for Turbulent Flow of Dilute Solutions of Drag-Reducing Polymers," Physics of Fluids (to be published, 1974).
- Jackson, D.A., and Paul, D.M. "Measurement of Supersonic Velocity and Turbulence by Laser Anemometry." Journal of Physics E. (Scientific Instrumentation) 4 (1971): 173-177.
- Jenkins, Francis A., and White, Harvey E. Fundamentals of Optics. New York: McGraw-Hill Book Company, Inc., 1957.
- Keller, A.; Yilmaz, E.; and Hammitt, F.G. Comparative Investigations of the Scattered Light Counting Method for the Registration of Cavitation Nuclei and the Coulter Counter. (University of Michigan, Department of Mechanical Engineering, Report No. UMICH 01357-36-T) Ann Arbor, Michigan, 1974.
- Kumor, Stanley M., and Sylvester, Nicholas D. "Effects of a Drag-Reducing Polymer on the Turbulent Boundary Layer," AIChE Symposium Series 130 69:1 (1973): 1-13.
- Lumley, J.L. "The Toms Phenomenon: Anomalous Effects in Turbulent Flow of Dilute Solutions of High Molecular Weight Linear Polymers," Applied Mechanics Review 20:1139 (1967).
- Mazumder, M.K.; McLeod, P.C.; and Testerman, M.K. Application of a Laser Doppler Velocity Meter in Turbulence Characterization, in The Use of the Laser Doppler Velocimeter for Flow Measurements. (Proceedings from a workshop at Purdue University, March 1972).
- Mazumder, M.K., and Wankum, D.L. "SNR and Spectral Broadening in Turbulence Structure Measurement Using a CW Laser," Applied Optics 9:3 (March 1970): 633-637.
- Roberts, David J. "Evaluation of a Laser Anemometer for Turbulence Measurements," (Case Western Reserve University, Department of Chemical Engineering, Research Report No. 01-04-74) Cleveland, 1974.
- Rudd, M.J. "A New Theoretical Model for the Laser Dopplermeter," Journal of Scientific Instruments (Journal of Physics E) 2:2 (1969): 45-48.
- Rudd, M.J. "Velocity Measurements Made with a Laser Dopplermeter on the Turbulent Pipe Flow of a Dilute Polymer Solution," Journal of Fluid Mechanics 51:4 (1972): 673-685.
- Sandborn, V.A. "Experimental Evaluation of Momentum Terms in Turbulent Pipe Flow," NACA TN 3266 (1955): 1-40.

Seyer, P.A., and Metzner, A.B. "Turbulence Phenomena in Drag Reducing Systems," AIChE Journal 15:3 (May 1968): 426-434.

Signetics Digital, Linear, Mos Applications Manual. Sunnyvale, California: Signetics Corporation, 1973.

Stevenson, W.H., and Thompson, H.D. chairmen and editors. Second International Workshop on Laser Velocimetry. (Proceedings of a workshop at Purdue University, March 1974).

Sylvester, Nicholas D., and Kumer, Stanley M. "Degradation of Dilute Polymer Solutions in Turbulent Tube Flow," AIChE Symposium Series 130 69 (1973): 69-81.

Tanner, R.I., and Pipkin, A.C. "Intrinsic Errors in Pressure-Hole Measurements," Transactions of the Society of Rheology 13:4 (1969): 471-484.

Virk, P.S.; Mickley, H.S.; and Smith, K.A. "The Ultimate Asymptote and Mean Flow Structure in Toms' Phenomenon," (Transactions of the ASME, June 1970) Journal of Applied Mechanics (1970): 488-493.

Walsh, M. "Theory of Drag Reduction in Dilute High-Polymer Flows," International Shipbuilding Progress 14 (1967): 134-139.

Walters, R.R. Drag-Reducing Polymer Molecular Weight Effects on Turbulent Diffusion for Uniformly Distributed Polymer Injection. (Advanced Technology Center Inc., Report No. B-94300/4CR-11) Dallas, Texas, March 1974.

Willmarth, W.W., and Lu, S.S. "Structure of the Reynolds Stress Near the Wall," Journal of Fluid Mechanics 55:1 (1972): 65-92.

Wilnhurst, T.H. "A Signal Simulator for Testing Laser-Doppler Fluid-Flow Velocimeter Systems," Journal of Physics E: Scientific Instruments 5 (1972): 1205-1208.

Yeh, Y., and Cummins, H.Z. "Localized Fluid Flow Measurements with an He-Ne Laser Spectrometer," Applied Physics Letters 4 (1964): 176-178.